Project ID: 2020-WSU-08

Quantifying and Reducing Uncertainty in Resilience Assessment of Transportation Networks Using Dynamic Bayesian Network

Final Report

By
Ji Yun Lee, Assistant Professor, Washington State University
Yue Li, Professor, Case Western Reserve University
Vishnupriya Jonnalagadda, Ph.D. Candidate, Washington State University

for

National University Transportation Center TriDurLE
Department of Civil & Environmental Engineering
405 Spokane Street PO Box 642910
Washington State University Pullman, WA 99164-2910

Date
4/29/2023

Acknowledgments

The work presented in this report was sponsored by the National Center for Transportation Infrastructure Durability & Life Extension (TriDurLE). This support is gratefully acknowledged. The authors also express their gratitude towards the individuals who served as a postdoctoral researcher (Dr. Seyed Hooman Ghasemi) and graduate students (Dr. Jie Zhao and Ms. Vishnupriya Jonnalagadda) and provided valuable assistance in this work.

Disclaimer

Table of Contents

List of Figures

List of Tables

Executive Summary

The Nation's transportation systems are complex and are some of the highest-valued and largest public assets in the United States. As a result of repeated natural hazards and their significant impact on transportation functionality and socio-economic health of communities, transportation resilience has gained increasing attention in recent years. Previous studies on transportation resilience have heavily emphasized network functionality during and/or following a scenario hazard event by implicitly assuming that sufficient knowledge of structural capacity and environmental/service conditions is available at the time of an extreme event. However, such assumptions often fail to consider the uncertainties that arise when an extreme hazard event occurs far into the future. Thus, it is essential to quantify and reduce uncertainties to better prepare for extreme events and accurately assess transportation resilience. By doing so, transportation systems can be better designed, maintained, and operated to mitigate potential damages and ensure the continuity of essential service during and after extreme events.

The goal of this project is to develop a dynamic Bayesian network (BN) based resilience assessment model for a large-scale transportation system that can quantify uncertainties and investigate the role of monitoring and inspection in uncertainty reduction. The project aims to better understand transportation system performance during normal and disrupted conditions, ultimately mitigating consequences from natural hazards. To achieve this goal, the project focuses on several tasks, including the formulation of a dynamic BN to update major random variables involved in resilience assessment over time, use of information entropy to quantify uncertainty, investigation of the role of monitoring and inspection data in reducing uncertainty, proposal of a dynamic BN-based model to assess the time-dependent resilience of a transportation system, and demonstration of the proposed model using a benchmark problem – a highway network in South

Carolina. The results of this project include the dynamic BN-based resilience assessment model, quantification of uncertainties at every stage of the model, and sensitivity analysis results that demonstrate the effectiveness of various inspection/monitoring techniques in reducing uncertainties. These results can be used to prioritize inspection and monitoring efforts and ensure that resources are allocated to the most effective techniques.

The potential impact of this project is significant as it offers decision-makers the tools and knowledge to better manage the resilience of transportation systems, particularly in the face of natural and man-made hazards. With the recent development of a wide range of monitoring and inspection techniques, including non-destructive testing, health monitoring equipment, satellite imagery, LiDAR, etc., the model, tools, and results of this project can be useful in determining which techniques to prioritize for implementation, evaluating the effectiveness of current monitoring/inspection programs, and performing the cost-benefit analysis of different techniques for optimal resource allocation.

Chapter 1. Introduction

1.1 Problem Statement

Decisions aimed at ensuring the adequate performance and operational integrity of transportation systems have strong implications for the health and economic well-being of the communities that they serve. Since their disruptions would have detrimental effects on the continuous flow of people, essential goods, and vehicles, and, in turn, economic security, transportation systems are generally expected to maintain prescribed minimum levels of service under normal and even disturbed conditions. Specifically, during and following man-made and natural hazards (e.g., bomb blasts, explosions, earthquakes, hurricanes, wildfires), transportation systems play a key role in providing access to the affected regions by rescuing people and transporting lifeline supplies (Zhou et al., 2019).

Due to the frequent occurrences and grave consequences of natural disasters in recent years, research pertaining to the resilience assessment of transportation systems has received a great deal of attention. Resilience for an engineered system is generally defined as its capacity to withstand, adapt, and recover from disruptions to ensure performance and meet customer demand (Bruneau et al., 2003; Chang and Shinozuka, 2004; Bruneau & Reinhorn, 2006; Madni & Jackson, 2009; Meerow et al., 2016; Bostick et al., 2018). Since there has been no widely accepted measure of resilience for transportation systems, researchers have proposed to define and quantify such resilience in different manners. These metrics are generally divided into topological metrics (Berche et al., 2009), attributes-based metrics (Murray-Tuite, 2006), and performance-based metrics (Bruneau et al., 2003). Although resilience capacities can be classified into absorptive, adaptive, and restorative capacities (Vugrin et al. 2011) according to the definition of resilience, most of the abovementioned metrics capture only one or two of the resilience capacities of a

system.

In recent years, some researchers have attempted to account for all capacities of resilience and have considered a series of resilience-enhancing strategies at multiple stages. For example, Miller-Hooks et al. (2012) formulated a two-stage stochastic integer program to measure and maximize the resilience level of a United States intermodal container network. This study incorporated both preparedness decisions and post-disaster recovery actions in order to achieve an optimal balance between pre- and post-disaster investment. Zhang et al. (2018) proposed a stage-wise decision framework that considers pre-disaster mitigation (Stage I), post-disaster emergency response (Stage II), and long-term recovery actions (Stage III). This study measured the performance of roadway networks in terms of their robustness, redundancy, and recoverability at each stage and formulated a stochastic multi-objective optimization problem to support resilience planning for roadway networks subjected to a scenario earthquake. However, these works provided a snapshot of system resilience after the realization of a scenario hazard event, ignoring the uncertainties in this scenario event as well as system resistance. Ouyang et al. (2012) introduced a time-dependent expected annual resilience metric, which combined a series of resilience-based improvement strategies and the associated attributes of resilience, in a three-stage (i.e., disaster prevention, damage propagation, and assessment and recovery) analytic model. In contrast to the previously mentioned studies, this metric explicitly considered uncertainties in potential hazards in analyzing infrastructure resilience.

While uncertainty quantification and reduction in life-cycle resilience assessment are essential to ensuring cost-effective resilience-enhancing strategies, many studies that propose a new resilience metric or resilience-based decision framework do not investigate the role of inspection/monitoring programs. One reason for this is that, as described above, most metrics or frameworks measure

scenario-based static resilience assuming that, at the time of hazard event occurrence, the full probabilistic descriptions of structural capacity and external loadings are known. However, there are substantial uncertainties in (a) the occurrence time and severity of a hazard event, (b) structural capacity in the future, and (c) external/service loadings especially when climate change affects the performance of an asset or when traffic demands change significantly as a result of population growth and urbanization. In recent years, transportation agencies have also realized the increasing uncertainties arising from aging and deteriorating infrastructure, increasing complexity of network, extreme events from natural and man-made hazards, budgets and resources, increasing operational demands among others. Failure to account for these factors and the associated uncertainties may affect the agency's capability to achieve its predefined goals and objectives. Moreover, if a resilience-based decision framework extends to a specified period of time and is intended to capture the time-dependent changes of structural performance and resilience, inspection/monitoring is necessary to increase the reliability of our prediction about structural capacity and/or external loadings in the future and ultimately transportation system resilience.

1.2 Objectives

Transportation systems are complex, and due to their connectivity, any damage to them would pose a significant threat to the well-being of the communities. To better understand transportation system performance during normal and disrupted conditions and ultimately mitigate consequences from natural and man-made hazards, it is critical to characterize uncertainties and reduce them through the efficient implementation of monitoring and inspection tools. To this end, this project develops a dynamic Bayesian network (BN) based resilience assessment model for a large-scale transportation system that can explicitly quantify uncertainties in all phases of the assessment and investigate the role of inspection and monitoring programs in uncertainty reduction. To achieve

this goal, the following tasks are performed in this project.

- Formulate dynamic BNs to update major random variables involved in transportation system performance assessment
- Investigate the role of monitoring and inspection programs in reducing uncertainty existing in resilience assessment, with a particular focus on various programs with different reliability
- Propose a dynamic BN-based model that assesses the time-dependent seismic resilience of a transportation system while identifying, quantifying, and reducing uncertainties explicitly
- Demonstrate the proposed model with a benchmark problem, a highway network in South Carolina

1.3 Expected Contributions

The contribution of this project is twofold. First, the proposed model can assess the time-dependent seismic resilience of a large-scale transportation system by characterizing uncertainties in all phases of resilience assessment, such as the number and time of hazard event occurrence, structural capacity in the future, and external/service loadings. Second, the role of monitoring and inspection programs in reducing uncertainties is investigated. In this project, monitoring/inspection equipment with a range of reliability is considered to study the sensitivity of the accuracy of system resilience estimation to data reliability. The results from this project can be used as comprehensive decision support information so that decision-makers (e.g., state Department of Transportation (DOT) risk managers, executives, and program and project managers) can have better understanding on the resilience of a transportation system and associated uncertainties, prioritize inspection and monitoring efforts, and ensure that resources are allocated to the most effective

techniques.

1.4 Report Overview

The rest of this report is structured as follows. Chapter 2 summarizes existing studies on (a) transportation resilience assessment and (b) the use of BN in transportation risk and resilience assessment to identify the research gap in the existing literature. Following this, the methodology for a dynamic BN-based resilience assessment is introduced. This chapter describes in detail time-dependent seismic fragility curves, network analysis, resilience assessment process, and uncertainty quantification and propagation. The fourth chapter illustrates the proposed model with a benchmark problem, a highway network in South Carolina, and the results and discussion are presented in Chapter 5. Finally, we conclude with a general discussion of the findings of this project.

Chapter 2. Literature Review

2.1. Transportation Resilience Assessment

Due to the unprecedented nature of disasters and their massive consequences, the resilience of a transportation system has been extensively studied in the literature on various modes of transportation, such as waterways, roadways, airways, and railways. As this project develops a dynamic BN-based resilience assessment model for a large-scale roadway system, this chapter places more emphasis on the literature review of the resilience of a highway road network.

Many quantitative and qualitative methods have been developed in recent years to assess roadway network resilience. For example, Adams et al. (2012) proposed a set of criteria to qualitatively assess resilience when a road system was subjected to disruptive weather events. However, quantitative methods have been more prevalent in transportation engineering because of their ability to be coupled with transportation simulation and to provide a quantitative basis for effective decision-making. Quantitative transportation resilience metrics are generally divided into topological metrics, attributes-based metrics, and performance-based metrics. Topological metrics include but are not limited to an average degree, cyclicity, and network diameter. Attributes-based metrics include adaptability, safety, mobility, and recovery, while performance-based metrics often indicate travel time and/or costs. These metrics can be measured by analytical solutions, simulation models, data-driven models, optimization models, or probabilistic models. Specifically, optimization models are useful for solving traffic assignment problems and for optimizing preparedness and recovery activities/resources.

Murray-Tuite (2006) is considered one of the first attempts to specifically define and quantitatively assess resilience in the context of transportation systems (Zhou et al., 2019). Murray-Tuite (2006)

stated that the use of multiple metrics and simulation techniques could provide a promising approach to addressing the complexity of resilience and defined ten dimensions of transportation resilience. The dimensions included redundancy, diversity, efficiency, autonomous components, strength, adaptability, collaboration, mobility, safety, and the ability to recover quickly (Murray-Tuite, 2006). These dimensions and their definitions are summarized in Table 1. To measure transportation resilience, Murray-Tuite (2006) evaluated only four out of the ten dimensions, that were adaptability, safety, mobility, and recovery, by using traffic assignment simulation methodology DYNASMART-P. Ip and Wang (2009) utilized the weighted average number of reliable independent paths in the road network to quantitatively measure the resilience of transportation networks. Cox et al. (2011) provided operational metrics to evaluate different aspects of transportation system resilience (e.g., vulnerability, flexibility, and resource availability) under terrorist attacks. With an emphasis on enhancing the resilience of a transportation network, Liao et al. (2018) aimed to measure and optimize transportation resilience under disasters. They considered three performance measurements (i.e., coping capacity, robustness, and flexibility) in evaluating transportation resilience.

Table 1. Dimensions of transportation resilience (adopted from Murray-Tuite, 2006)

Dimension	Definition
Redundancy	Redundancy indicates that multiple components serve the same function.
Efficiency	Efficiency indicates input-output ratio optimization.
Diversity	Diversity means that the components are functionally different.
Strength	Strength indicates the system's ability to withstand an event.
Adaptability	Adaptability implies that the system is flexible, and elements are capable of learning from past experiences.
Autonomous components	Autonomous components can operate independently.
Collaboration	Collaboration indicates that information and resources are shared among components or stakeholders.
Mobility	Mobility indicates that travellers can reach their chosen destinations at an acceptable level of service.
Safety	Safety suggests that the system does not harm its users or unduly

	expose them to hazards.
Recovery	The ability to recover quickly means that an acceptable level of service can be restored rapidly and with minimal outside assistance after an event occurs.

To study network topological characteristics and their role in transportation resilience, Zhang et al. (2015) proposed an optimization-based framework which considered throughput and connectivity in quantifying resilience and conducted numerical experiments on 17 different network structures by including preparedness and recovery activities. The results provided a basis for characterizing highly resilient network topologies and identifying network attributes that might lead to poorly performing systems. Ganin et al. (2017) stated that evaluating road networks based only on their operating state during normal conditions resulted in little information about system performance under disrupted conditions. By using observed data of annual delay per peak-period auto commuter, they developed an urban roadway efficiency model and used it to calculate resilience. They defined resilience as a change in efficiency resulting from roadway disruptions and applied their model to road transportation networks in 40 major US cities. The results showed that, under disruptive conditions, the failure of network components ultimately led to the failure of the entire network and suggested that it would be important to evaluate the significance of network components in prioritizing network resilience improvement activities. Barker et al. (2013) proposed two resilience-based component importance measures and defined resilience as a function of reliability, vulnerability, survivability, and recoverability. Modeling emphasis was placed on vulnerability and recoverability so that the results could help formulate resilience-enhancing activities such as vulnerability reduction activities and accelerated recovery processes. However, most of the previous studies on transportation resilience have focused on the effect of a single type of hazard on system performance in the immediate aftermath of such event and provided a snapshot of system resilience after the realization of a scenario hazard event. While

some existing studies have considered uncertainties in this scenario event as well as system resistance, they still have not addressed the effects of multiple risk factors that may occur over a longer-term planning horizon. To address this research gap, in our recent study, multiple risk factors and opportunities were considered in resilience assessment (Zhao et al., 2022). We first identified and classified multiple risk factors into various categories based on their effects on transportation system functionality and evaluated their combined effect on long-term system performance through integrated risk assessment. Then, we developed a multi-component resilience index to measure the capability of a transportation system subjected to multiple risk factors. The proposed multi-component resilience index was designed to properly account for and manage various risk factors in the resilience planning of a transportation network. Finally, we used the proposed resilience index for a state highway system in the state of Washington and concluded that the combined effect of various risk factors was important in better understanding system capability and ultimately improving its resilience. While uncertainties in risk factors were considered in the proposed multi-component resilience assessment, uncertainties were not explicitly characterized, tracked, or reduced in the process.

2.2. Use of Bayesian Network in Transportation Risk and Resilience Assessment

In the process of resilience evaluation, there are substantial uncertainties involved as much information is not available regarding disruptive events. Moreover, these events occur sometime far into the future. This makes probabilistic methods suitable because these methods can quantify uncertainties through stochastic descriptions of resilience and its measures. Some studies have used probabilistic methods, and a number of researchers have proposed the usage of BN for the evaluation of transportation resilience. BN is a graphical model that permits the design of

stochastic relationships among a group of variables. BN models are also used to update the prior probabilities of a random variable when some information describing the variable becomes available. However, considering subjective information in the form of expert knowledge and surveys to define the relationships among the variables in BN can lead to the improper quantification of uncertainties.

John et al. (2016) presented a resilience assessment approach that employed BN to model various influencing variables in a seaport system. The study showed that the proposed methodology could provide safety analysts with a useful tool to implement strategies that would contribute to the resilience enhancement of maritime systems. Hosseini and Barker (2016) offered a methodology to quantify resilience as a function of absorptive, adaptive, and restorative capacities of resilience using BNs. BN was used in their study to track and quantify uncertainty propagation and ultimately improve resilience-enhancing decision-making. They applied their model to an inland waterway network and demonstrated how sensitivity analyses could help pre- and post-disaster strategies for building the resilience of the system. Castillo et al. (2016) presented a BN-based model for probabilistic risk assessment of railway lines. In their model, they attempted to reduce the complexity of the problem as railway lines in the real world have variables as high as thousand or more. To achieve this goal, they divided the BN into small parts such that the complexity of the problem would become linear in the number of items and subnetworks. Additionally, the application of the backward inference process of BN helped identify the causes when an accident occurred. Quantification of resilience is complex given the fact the performance and recovery process vary from location to location and are region-specific. Thus, Kanti Sen and Dutta (2020) presented an integrated Geographic Information System (GIS)-Bayesian Belief Network (BBN) framework to model and quantify the resilience of network infrastructure systems against flood

hazards. They stated that the proposed framework could be generalized and valid for other hazard types and other types of infrastructure systems.

While transportation resilience is often dynamic due to the evolving nature of external and internal factors affecting transportation performance, most of the abovementioned studies considered resilience as a static one and employed static BN. Kammouh et al. (2020) presented both static and dynamic BN frameworks to evaluate the resilience of engineering systems. The dynamic BN extends the classical BN by adding a time dimension. The proposed resilience framework was presented in the form of a mathematical formulation that integrated the probability distributions of all variable states. The static BN framework was applied to evaluate the resilience of the country Brazil against natural and manmade disasters, while the dynamic BN framework was used to evaluate the resilience of a transportation system. Their study showed that the dynamic BN framework better performed in dynamically modeling complex systems even in cases where data were scarce. In summary, BN has been used extensively in the literature to assess the risk and resilience of complex engineering systems due to its ability to represent conditional dependencies between a set of variables. Specifically, the aspects of BN like the forward and backward propagation are highly successful in decision making in the face of uncertainty.

2.3. Summary

From the literature review, most studies on transportation resilience have thoroughly emphasized network functionality during and/or following a scenario hazard event by implicitly assuming that sufficient knowledge of structural capacity and environmental/service conditions is available at the time of an extreme event. However, it is identified that such knowledge often involves uncertainties, and thus uncertainties should be quantified and properly managed to improve the accuracy of resilience assessment. Moreover, only a few studies have considered the

interdependencies between random variables in the assessment model. One way of addressing this issue is to embed BN in resilience assessment model to quantify uncertainties in (a) the number and time of hazard event occurrence, (b) hazard severity, (c) structural capacity over time, (d) external/service loadings, and (e) the availability of repair resources that may affect the resilience capacities of transportation system not only at the present time but also in the future. Furthermore, it is important to include the effect of monitoring and inspection activities throughout the lifecycle of transportation system, aimed at reducing uncertainties and improving the accuracy of resilience assessment. To address the research gaps identified in this chapter, we propose a transportation resilience assessment model where dynamic BN and information entropy are used to quantify and reduce uncertainties in resilience-related random variables while formulating interdependencies between these variables.

Chapter 3. Methodology

From the literature review, it has been identified that many existing studies have not explicitly considered and quantified uncertainties involved in the calculation of the resilience of a highway network. Moreover, little studies have investigated the role of inspection and monitoring programs in reducing uncertainties associated with key parameters in resilience assessment. This chapter proposes a model that quantifies and reduces uncertainties along the process of seismic resilience assessment through information entropy and dynamic BN. Figure 1 shows the overall resilience of a highway network subjected to a scenario hazard event (e.g., M 6.8 scenario earthquake). In the proposed model, it is assumed that uncertainties exist at all stages of the resilience assessment procedure as described by the probability distribution functions (PDFs) in Figure 1. While the functionality of the highway network is measured by the total travel time, seismic resilience is measured by the area above the recovery trajectory curve in the aftermath of the event.

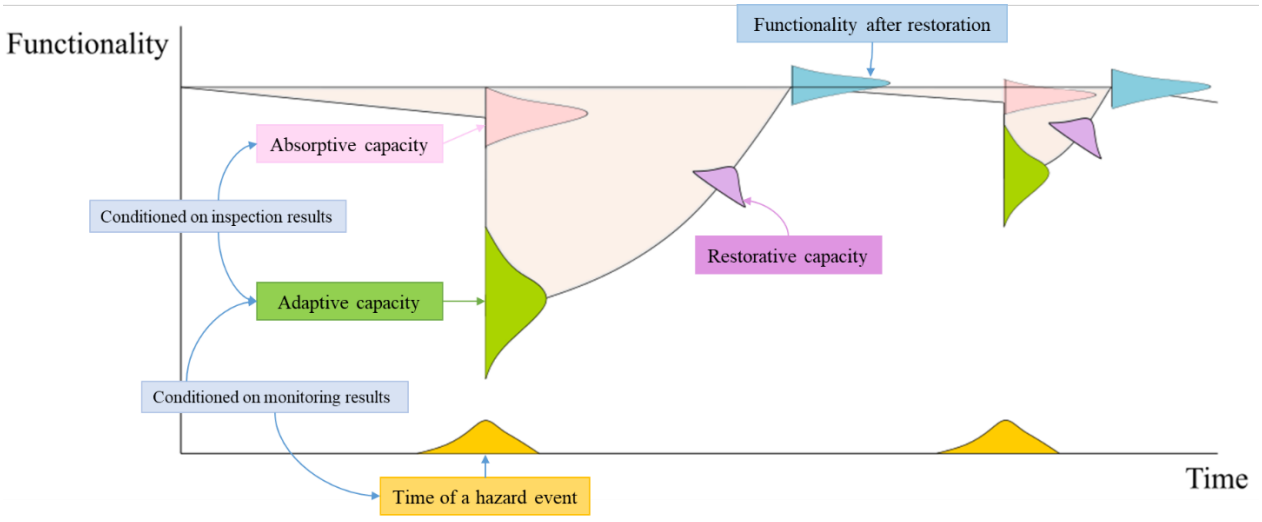

Figure 1. Uncertainties at different stages of the proposed model

As illustrated in Figure 2, the model begins by measuring the time-dependent structural reliability of individual bridges exposed to corrosion (Section 3.1) and linking this measure to post-earthquake traffic carrying capacity (Section 3.2). Then, the performance of individual bridges is

aggregated through network analysis to evaluate the performance of the highway network in terms of total travel time or cost prior to and following a hazard event (Section 3.3). By incorporating time-dependent restorative activities into the network analysis, the network seismic resilience is assessed (Section 3.4). In the meantime, the PDFs of bridge and network functionalities are updated based on inspection and monitoring data over time through dynamic BN. Finally, information entropy is used to quantify uncertainties in seismic resilience index and to study the sensitivity of the seismic resilience index to the reliability of inspection and monitoring data (Section 3.5). Figure 2 shows the overall flowchart of the proposed dynamic BN-based seismic resilience assessment of a highway network.

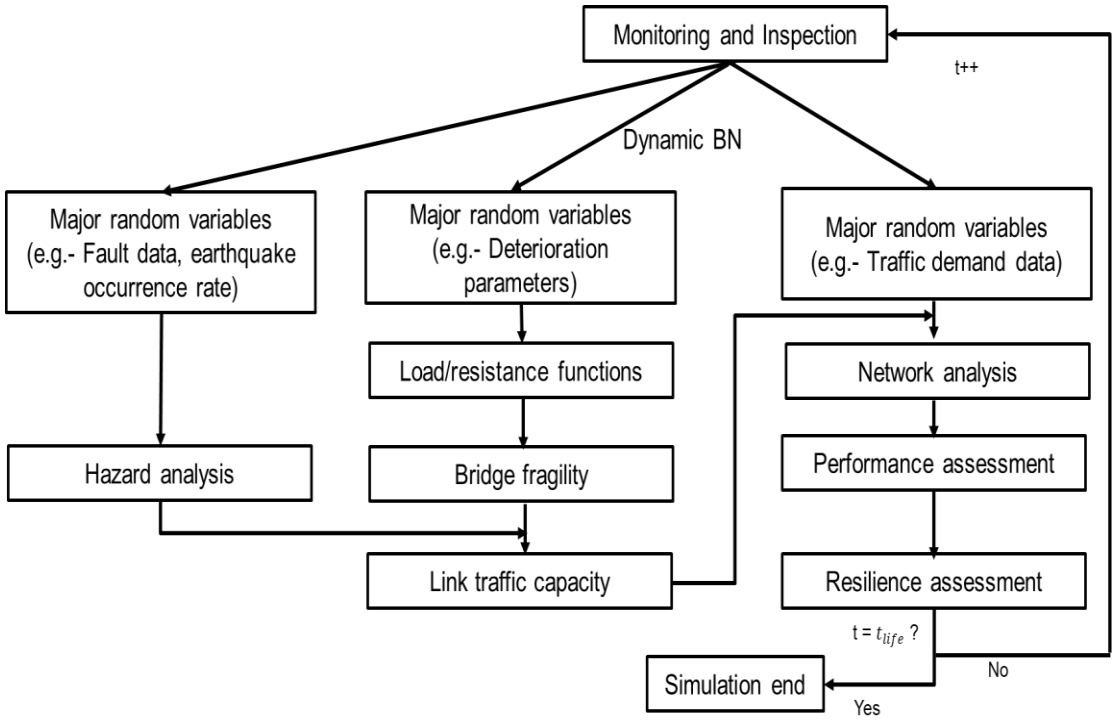

Figure 2. Flow chart showing a procedure for the proposed model

3.1 Time-dependent Structural Reliability Assessment of Bridges Exposed to Corrosion

Bridges are one of the most critical elements in a transportation network, and based on past experiences (e.g., the 1994 Northridge earthquake, the 1995 Kobe earthquake, the 1999 Chi-Chi earthquake, the 2011 Tohoku earthquake, etc.), they are perceived as one of the most vulnerable components that may experience significant structural damage in the event of earthquakes (Frangopol & Nakib, 1991; Mackie and Stojadinovic, 2006; Padgett & DesRoches, 2007; Shiraki et al., 2007). Thus, in this project, we focus on the post-earthquake performance of individual bridges in assessing the seismic resilience of a highway network. The absorptive capacity (or robustness) of a bridge is the capability to absorb the shock of the disruption, which is an inherent feature and is considered the first course of defense in response to an earthquake event. This subsection illustrates how the absorptive capacity of a bridge changes over time especially when it is exposed to corrosion.

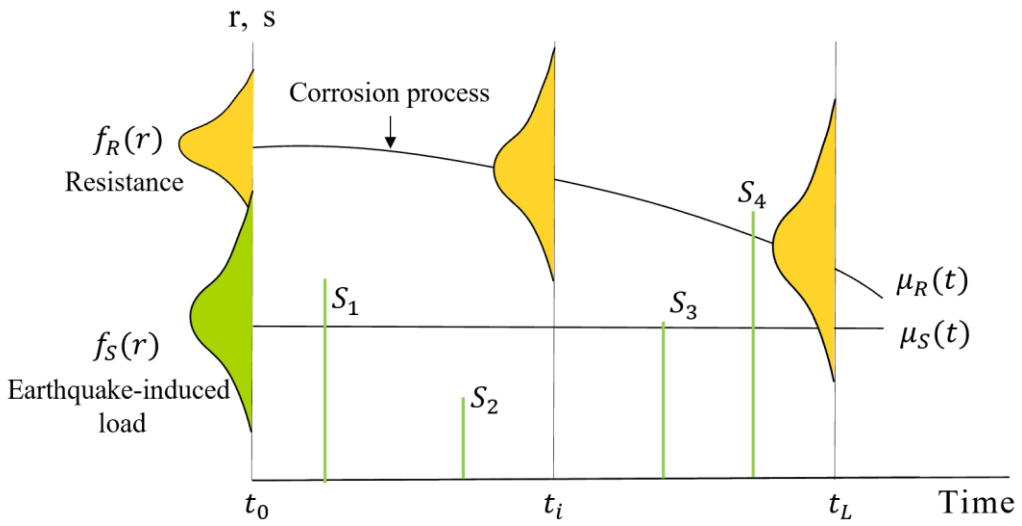

Figure 3. Time-dependent performance profile of a bridge exposed to both earthquake loads and corrosion

Bridges in coastal environments or cold climates are exposed to chloride-induced corrosion, which is known to be a major cause of structural deterioration. As shown in Figure 3, a bridge slowly loses its capacity to resist extreme loading over time due to corrosion and therefore has a higher

probability of failure when being subjected to earthquakes. Time-dependent reliability (i.e., the probability that the limit state of a bridge will not be exceeded) is modeled by incorporating time-dependent deterioration in structural elements.

For a reinforced concrete (RC) member, chloride accumulation profiles in concrete can be modeled by using the Fick's second law (Atadero et al., 2019; Gong & Frangopol, 2020; Bu et al., 2022):

$$C(x,t) = C_s\left(1 - erf\frac{x}{2\sqrt{D_c t}}\right) \tag{1}$$

where $C(x,t)$ = the chloride concentration at a distance x (m) from the surface at time t (kg/m^3); C_s = the chloride concentration at the surface (kg/m^3); erf = the gaussian error function; and D_c = the diffusion coefficient (m^2/year). By setting $C(x,t)$ equal to the critical chloride concentration (C_{cr}), Equation 1 can be solved for t. Then, the corresponding corrosion initiation time, T_i, is calculated by (Thoft-Christensen et al., 1996):

$$T_i = \frac{x^2}{4D_c}\left[erf^{-1}\left(\frac{C_s - C_{cr}}{C_s}\right)\right]^{-2} \tag{2}$$

Once corrosion initiates, the reinforcement diameter decreases over time and can be mathematically expressed by a time-dependent function:

$$D(t) = D_0 - r_{corr}(t - T_i) \tag{3}$$

where $D(t)$ = the reinforcement diameter at time t; D_0 = the initial diameter of a reinforcing rebar; and r_{corr} = the rate of corrosion. Consequently, the remaining cross-sectional area of reinforcement can be estimated by the following expressions (Stewart & Rosowsky, 1998):

$$A(t) = \begin{cases} nD_0^2\frac{\pi}{4} & for\ t \le T_i \\ n[D(t)]^2\frac{\pi}{4} & for\ T_i < t < T_i + D_i/r_{corr} \\ 0 & for\ t \ge T_i + \frac{D_i}{r_{corr}} \end{cases} \tag{4}$$

in which n = the number of reinforcing rebars.

In addition, the corrosion of reinforcement also results in the reduction of strength of rebars and concrete. The residual capacity of corroded reinforcing steels could be estimated by the regression model proposed by (Du et al., 2005):

$$f_{y,cor} = \left(1.0 - \beta_y Q_{corr}\right) f_y \tag{5}$$

where $f_{y,cor}$ and f_y = the yield strengths of corroded and non-corroded reinforcement, respectively; Q_{corr} = the amount of corrosion of reinforcement (%) in terms of weight loss; and β_y = the attenuation coefficients of yield strength of rebars, which is taken as 1.24 for uniform corrosion of steel reinforcement according to the experiment conducted by Lee and Cho (2009).

Meanwhile, due to the corrosive expansion of steels, the surrounding concrete will yield microcracking, and compressive strength also decreases. The reduced concrete strength can be calculated as the follows (Coronelli & Gambarova, 2004):

$$f_{c,corr} = \frac{f_c}{1 + K\frac{\varepsilon_1}{\varepsilon_{\mathrm{co}}}} \tag{6}$$

where $f_{c,corr}$ = the compressive strength of concrete after corrosion and cracking; f_c = the compressive strength of concrete without cracking; K = the coefficient related to bar roughness and diameter; $\varepsilon_{\mathrm{co}}$ = the strain at the peak compressive stress; and ε_1 = the average tensile strain in the cracked concrete at right angles to the direction of the applied compression. The strain ε_1 is evaluated by means of Equation 7:

$$\varepsilon_1 = \left(b_f - b_0\right)/b_0 \tag{7}$$

where b_0 = the section width in the virgin state (no corrosion cracks); and b_f = the beam width increased by corrosion cracking. An approximation of the increase of the beam width is given by:

$$b_f - b_0 = n_{\mathrm{bars}} w_{cr} \tag{8}$$

where n_{bars} = the number of the rebars in compression layer; and w_{cr} = the total crack width for a given corrosion level X to be evaluated—for instance—by using the relation proposed by Molina et al. (1993):

$$w_{cr} = \sum_{i} u_{i,\text{corr}} = 2\pi(v_{rs}-1)X \tag{9}$$

where $u_{i,\text{corr}}$ = the opening of each single corrosion crack; v_{rs} = the ratio of volumetric expansion of the oxides with respect to the virgin material, taken as 2 (Molina et al. 1993); and X = the depth of the corrosion attack. The mechanical behavior of steel reinforcement and concrete under corrosion attack considered in this study are shown in Figure 4(a) and Figure 4(b), respectively, where the shift of the mechanical behavior of cracked concrete cover refers to compression softening model proposed by Vecchio and Collins (1993).

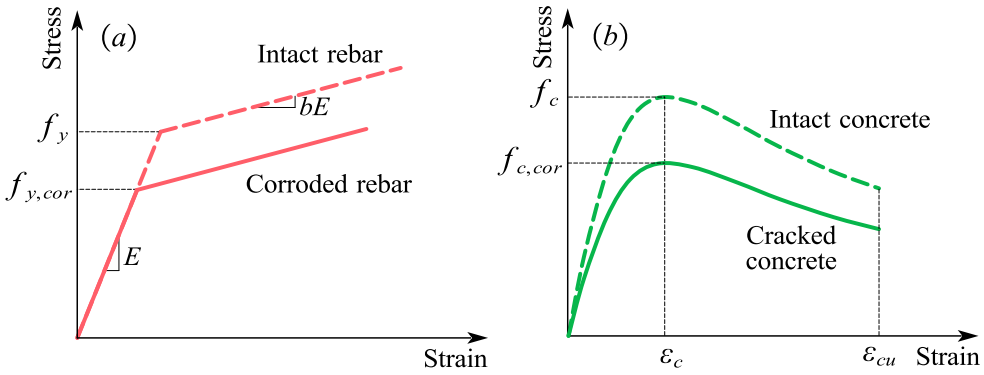

Figure 4. Schematic diagram of constitutive models with and without corrosion effects: (a) reinforcing steel and (b) concrete

For a steel girder bridge, uniform deterioration is the dominant form of corrosion deterioration and is typically used to calculate steel deterioration (Czarnecki & Nowak, 2008). The corrosion depth on steel girders can be estimated by power-law (Naeemi & Albrecht, 1984):

$$d_s(t) = a\left(t - T_{gc}\right)^b \tag{10}$$

where a and b = the model coefficients; and T_{gc} = the coating service life of the girder. Additionally, other bridge elements (e.g., elastomeric bearing pads and steel bearing anchor bolts) are also subject to aging and experience structural deterioration.

The failure probability of a component or system is computed by Equation 11:

$$P_f(t) = \int_0^{\infty}\left(\int_0^{S} f_{R,S}(t)dr\right)ds \tag{11}$$

where $P_f(t)$ = the failure probability of a component or system; and $f_{R,S}(t)$ = the joint probability distribution of resistance (R) and load (S) functions. Since structural deterioration due to corrosion reduces the strength of a component or system over time, time-dependent failure probability will be estimated by accounting for the effects of corrosion deterioration in the resistance model.

In this project, we adopt the parameterized seismic fragility model proposed by Ghosh (2013) to assess the time-dependent failure probabilities of bridges. It is because (a) this model can reduce substantial computation burden by replacing a large number of nonlinear dynamic analyses of complete finite element models with a surrogate model (Ghosh et al., 2014); (b) it can capture time-dependent deterioration in the structural elements; and (c) it can incorporate new observed data obtained from field measurement instrumentation and update the probabilities of bridges. The parameterized seismic fragility curve equation is generally expressed by (Ghosh et al., 2014):

$$P_{sys|im,x_1,x_2,\ldots..x_m} = P\left[bin_{sys,i} = 1 \middle| im, x_1, x_2, \ldots, x_m\right] = \frac{e^{\theta_{sys,0}+\theta_{sys,im}im+\sum_{j=1}^{m}\theta_{sys,j}x_j}}{1+e^{\theta_{sys,0}+\theta_{sys,im}+\sum_{j=1}^{m}\theta_{sys,j}x_j}} \tag{12}$$

in which $P_{sys|im,x_1,x_2,\ldots..x_m}$ = the conditional probability of system-level failure; im = the intensity of ground motions; $\boldsymbol{x}$ = the set of m critical parameters affecting the seismic performance of the deteriorating bridge; bin = the binary vector indicating either system survival (bin = 0) or system failure (bin = 1), $\boldsymbol{\theta}$ = the set of logistic regression coefficients. Table 2 shows an example of the input vector $\boldsymbol{x}$ consisting of deterioration-affected structural parameters and critical bridge

modeling parameters of a multi-span continuous (MSC) concrete box girder. The vector $\boldsymbol{x}$ and their values vary depending on bridge component and types.

Table 2. Elements of the input vector $\boldsymbol{x}$ of a multi-span continuous concrete box girder

Elements in vector $\boldsymbol{x}$	Parameter description	Units	Values assumed based on Ghosh (2013)
x_1	Area of rebar	cm^2	Equation 4
x_2	Elastomeric bearing dowel bar area	cm^2	2.8145
x_3	Shear modulus of elastomeric bearing pads	Mpa	3.05
x_4	Abutment gap	cm	1
x_5	Concrete cover depth	cm	6

To reduce uncertainties involved in structural deterioration process, the deterioration parameters (e.g., C_s, D_c, and r_{corr}) can be monitored through field instrumentation and used to update the input vector $\boldsymbol{x}$ through BN. Ultimately, the updated input vectors are incorporated into the parameterized fragility curve to update the probability of failure. This procedure will be illustrated in more detail in Section 3.5.

3.2 Post-earthquake Traffic Flow Capacity Assessment of Highway Bridges

Following an earthquake event, a bridge can be fully operational or can carry only some portion of the traffic load that can be safely carried by an intact bridge. Truck weight and speed restrictions or lane closures can be implemented to reduce the traffic load that needs to be carried by a damaged bridge. To assess the post-earthquake functionality of a bridge, in this subsection, we propose a methodology for linking the post-earthquake reliability index of a bridge to the resulting traffic flow capacity by adjusting the mean values of live load in reliability calculation (Ghasemi & Lee, 2021). After developing the relationship between the post-earthquake allowable traffic flow capacity and the associated reliability index, the post-earthquake reliability index obtained from

Section 3.1 can be used to find the associated allowable traffic flow capacity from the relationship. In Section 3.1, the probability of failure of an individual bridge given a specific ground motion intensity can be calculated by Equation 12. Then, the reliability index, β, of a bridge structure is calculated by:

$$\beta = \Phi^{-1}(1 - p_f) \tag{13}$$

where $\Phi^{-1}(\cdot)$ = the inverse of the cumulative distribution function of a standard normal random variable; and p_f = the probability of failure of the bridge. The relationship between β and traffic flow capacity (FC) is developed based on the working-backward method (Ghasemi & Lee, 2021). First, it is assumed that a bridge is designed based on different load combinations corresponding to different allowable traffic flow capacities. For example, as presented in Table 3, if a bridge is assumed to carry only half of the original traffic flow capacity, live load statistics ($L + DY$) in the load combination should be reduced by half, while other loads (i.e., dead load, (D) and wearing dead load (Dw)) remain the same. Accordingly, the required structural resistance to tolerate the assumed live load is expected to be reduced. Table 3 also shows the traffic FC and the associated load combination. The load combinations shown in Table 3 correspond to only strength limit state function, because the probability that the two severe earthquake events occur successively in a short time interval is negligible. Therefore, the extreme event limit state function and the associated load combination are not taken into account.

Table 3. Illustrative relationship between reliability index and traffic flow capacity

Traffic FC	Load Combination	β
Full	$1.25D + 1.5Dw + 1.75(L + DY)$	4.00
3/4	$1.25D + 1.5Dw + 0.75 \times 1.75(L + DY)$	3.15
1/2	$1.25D + 1.5Dw + 0.50 \times 1.75(L + DY)$	2.00
1/3	$1.25D + 1.5Dw + 0.33 \times 1.75(L + DY)$	0.85

1/4	$1.25D + 1.5Dw + 0.25 \times 1.75(L + DY)$	0.20

Note: D = the dead load; Dw = the dead load due to wearing surface; L = the live load; and IM = the dynamic load.

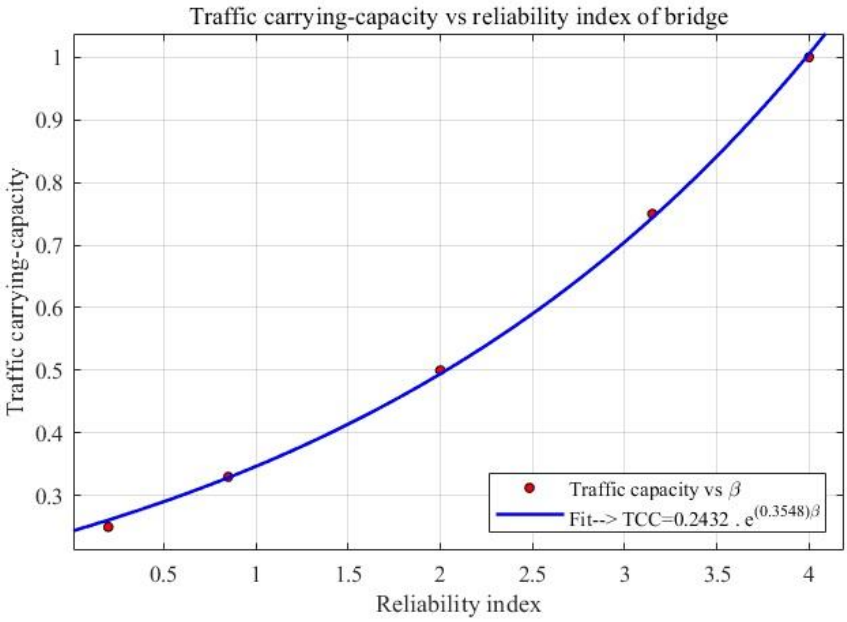

Figure 5. Continuous relationship between reliability index and traffic flow capacity

To compute the reliability indices associated with different load combinations, Monte Carlo simulation is performed for 36 different bridges by considering uncertainties in both resistance and loads. Statistical parameters of loads (i.e., D, Dw, and $L + DY$) are obtained from Nowak and Collins (2012), and uncertainties in resistance, which are related to the failure/fracture mode of component, are obtained from Ellingwood (1996). The reliability index of a bridge corresponding to each load combination is computed and presented in Table 3. The reliability indices shown in the last column of Table 3 represent the minimum reliability indices that are required to safely carry the partial traffic flow capacity shown in the first column of Table 3. Table 3 can now be used in reverse order. After finding the post-earthquake reliability index of a bridge, the corresponding allowable traffic flow capacity can be found using the relationship presented in

Table 3. In order to facilitate such use, the continuous relationship between β and FC is also constructed as illustrated in Figure 5. More detailed information on the procedure for deriving the relationship between traffic flow capacity and reliability index can be found in Ghasemi and Lee (2021).

3.3 Network Analysis: A Highway Network Involving Multiple Bridges

Adaptive capacity (or redundancy) is the ability of a transportation network to organize by itself to avoid any discontinuity of its performance and adapt to disruptions. Assuming that two systems are subjected to the same magnitude of an extreme event, the network having a higher adaptive capacity is more likely to experience less reduction in performance because the redundancy of the network (e.g., alternative routes) ensures the continuity of its performance. Thus, adaptive capacity is an inherent feature of the network and can be improved by ensuring alternative routes in the system. Future changes in traffic demand may affect the adaptive capacity of a network, and monitoring data on traffic demand are used in updating network redundancy and informing a better decision on alternative paths. Following an earthquake event, the absorptive capacities of all bridge structures are included in network analysis as illustrated in Figure 6, and network redundancy can be assessed during a distress situation.

Performance of the network can be evaluated in terms of total travel time or cost. Conventional connectivity reliability accounts only for two binary states of a link (full capacity or complete failure), which may mislead the actual performance of the network. On the other hand, travel time (and costs) can consider different levels of link capacities and incorporate dynamic traffic demand over time. Thus, travel time and cost are useful measures to determine network performance under traffic flow variation (Chen et al., 2013) and to be used in cost-benefit analysis to determine the effectiveness of the institutional investments in maintenance and repair activities in improving the

resilience of a road network.

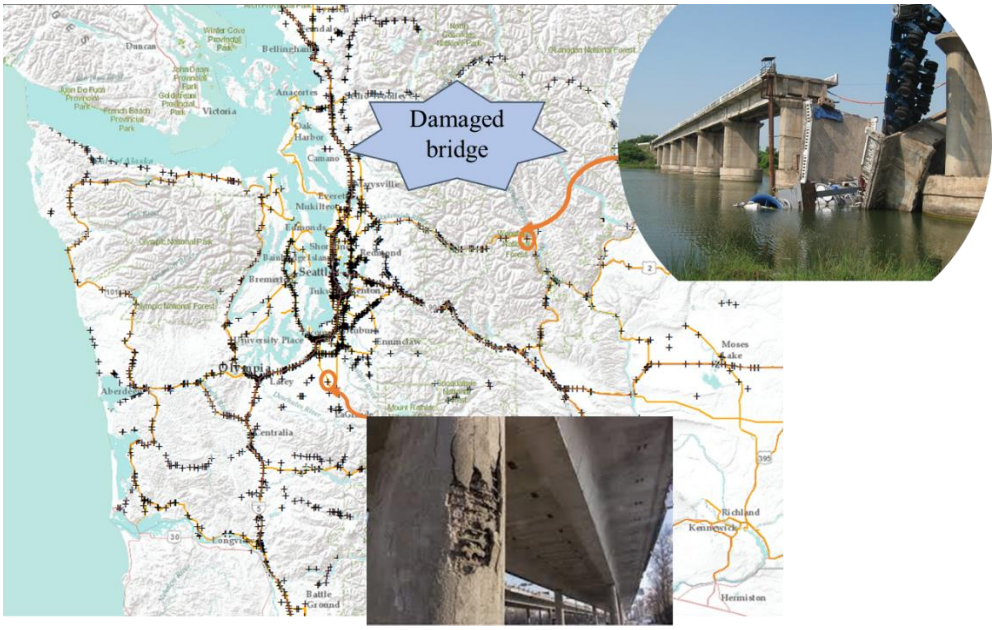

Figure 6. Incorporation of the performance of individual bridges into network analysis

To assess the post-earthquake performance of a highway network, first, a seismic hazard analysis is performed to simulate a scenario earthquake event. In this project, a ground motion intensity map is generated using OpenSHA to realize ground motion intensities at all bridge sites in the study region. Conditioned on the realized ground motion intensity, the failure probability of each bridge can be estimated based on a bridge seismic fragility curve (e.g., Equation 12). Then, Monte Carlo Simulation (MCS) is used to determine the damage state of each bridge. This process is coupled with ArcGIS and uses a Geographic Information System with data on bridges and highway segments in the United States.

Second, the post-earthquake reliability index of each bridge is determined using its seismic fragility curve (c.f., Equation 12), and subsequently, is used to compute the corresponding allowable traffic flow capacity using the relationship presented in Table 3 and Figure 5. If multiple bridges are located on the same link (i.e., the road segment between junctions), they are modeled as a series system, which indicates that the failure of a single bridge leads to link failure. The post-

earthquake traffic carrying capacities of all links in the study region are then combined with their corresponding traffic demands within network analysis to estimate post-earthquake network performance. In this paper, we assess highway network performance using CUBE voyager software program which enables macroscopic traffic simulation. This program requires network GIS data, the traffic capacity and demand at each link, and origin destination (O-D) pairs as major input data. During normal operations, the performance of the highway network is assessed by the aggregated travel time of the fastest routes between all O-D pairs. Following an earthquake event, post-earthquake link capacities obtained from the previous step are incorporated into the network analysis to determine the fastest routes between the same set of O-D pairs. The performance of the highway network is assessed at every time interval whenever new information on bridge reliability or link traffic demand becomes available.

3.4 Seismic Resilience Assessment of a Highway Network

This subsection illustrates the procedure for assessing the seismic resilience of a highway network. Although there is no single agreed upon indicator for measuring resilience, loss of resilience, R_{loss}, with respect to a specific earthquake event, has been widely used as a resilience indicator over the past two decades (Bruneau et al., 2003). As shown in Figure 7, the loss of resilience can be measured by the area above the post-earthquake recovery trajectories and accounts for both the expected degradation in quality and the recovery time. It is mathematically expressed by:

$$R_{loss} = \int_{t_0}^{t_1} [100 - Q(t)]\, dt \tag{14}$$

where t_0 = the time of occurrence of an earthquake event; t_1 = the time when a bridge/network is completely repaired; and $Q(t)$ = the time-dependent quality (or performance) of the structure. To improve the seismic resilience of the structure, R_{loss} should be reduced.

A similar formulation is adopted in this study. The seismic resilience of a highway network is

measured by the normalized area under the post-earthquake recovery trajectories and can be expressed as:

$$R = \frac{1}{t_1 - t_0} \int_{t_0}^{t_1} Q(t)\, dt \tag{15}$$

Contrary to R_{loss}, a higher value of R indicates a more seismically resilient network. In this project, network performance is expressed as a function of total travel time as follows (Kezhiyur, 2015):

$$Q(t) = 100 - 100 \left(\frac{TTT(t) - TTT_0}{TTT_0} \right) \tag{16}$$

where $TTT(t)$ = the total travel time at time t; and TTT_0 = the total travel time in the base model (measured without any disaster event).

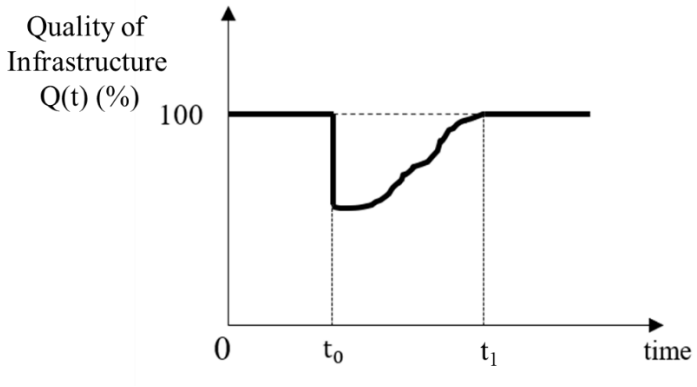

Figure 7. A conceptual representation of the time-dependent performance of a structure (adopted from Bruneau et al. (2003))

To capture both the time-dependent nature of resilience and uncertainty propagation, network resilience is assessed at every time step (e.g., 2 years) over a specified time period (e.g., 50 years) by assuming that a highway network is subjected to the same scenario earthquake event. Network resilience is expected to change due to time-dependent bridge reliability and traffic demand. However, due to substantial uncertainties in seismic resilience assessment, the estimated network resilience might be different from true network resilience. Thus, inspection and monitoring are performed continuously over time, and their results are incorporated in updating the stochastic

models of bridge fragility and link traffic demand through dynamic BN. Using the updated models, network resilience is estimated at every time step and is compared with the one estimated based only on prior information to investigate the role of inspection/monitoring programs in reducing uncertainties in seismic resilience assessment.

3.5 Uncertainty Quantification and Propagation in Resilience Assessment

This subsection illustrates the procedure for quantifying uncertainties and tracking their propagation from stochastic models to overall resilience assessment. There are two types of uncertainties – aleatory and epistemic. Aleatory uncertainties are defined as randomness or inherent variability of a physical phenomenon and thus are essentially irreducible. For example, wind speeds at a site are typically characterized by Weibull distribution. Additional sampling will not change its coefficient of variation in any significant way. On the other hand, epistemic uncertainties are knowledge-based and generally can be reduced with additional knowledge. Additional knowledge comes at a price and there is a trade-off between cost and uncertainty reduction. Thus, in this project, epistemic uncertainties are reduced by incorporating additional information obtained from inspection and field instrumentation through Bayesian updating.

BN has been widely applied in the field of reliability and resilience assessment due to its ability to update prior knowledge based on new observed data. BN is a reliable tool that accounts for the influence of uncertainty and variability to predict model outcomes for a complex system. Moreover, BN is capable of accounting for both quantitative and qualitative variables and handling missing data by considering the uncertainty within the system. In Bayes' Theorem, initial knowledge of a parameter (θ) is encoded in a prior PDF, $f(\theta)$. After incorporating observed data (d), a posterior PDF of the parameter, $f(\theta|d)$, is calculated by:

$$f(\theta|d) = \frac{f(d|\theta)f(\theta)}{f(d)} \tag{17}$$

where $f(d|\theta)$ = the likelihood function that quantifies the likelihood of observing this data given θ; and $f(d)$ = the marginal probability of the data. As such, the posterior PDF of the parameter is obtained by updating the prior PDF in light of the observed data and is more informative than the prior one if the data are sufficiently reliable.

As shown in Figure 8, major random variables related to corrosion, seismic hazards, and traffic demands can be monitored. In the proposed resilience assessment framework, the parameterized fragility curve equations (c.f., Equation 12) of individual bridges are continually updated based on field instrumentation data, while traffic count data, such as annual average daily traffic (AADT) data, are incorporated to update the prior PDF of traffic demand on each link. BN can be used to develop a series of probabilistic graphical models aimed at identifying the relative contributions of uncertainties at each stage to uncertainties in the overall resilience.

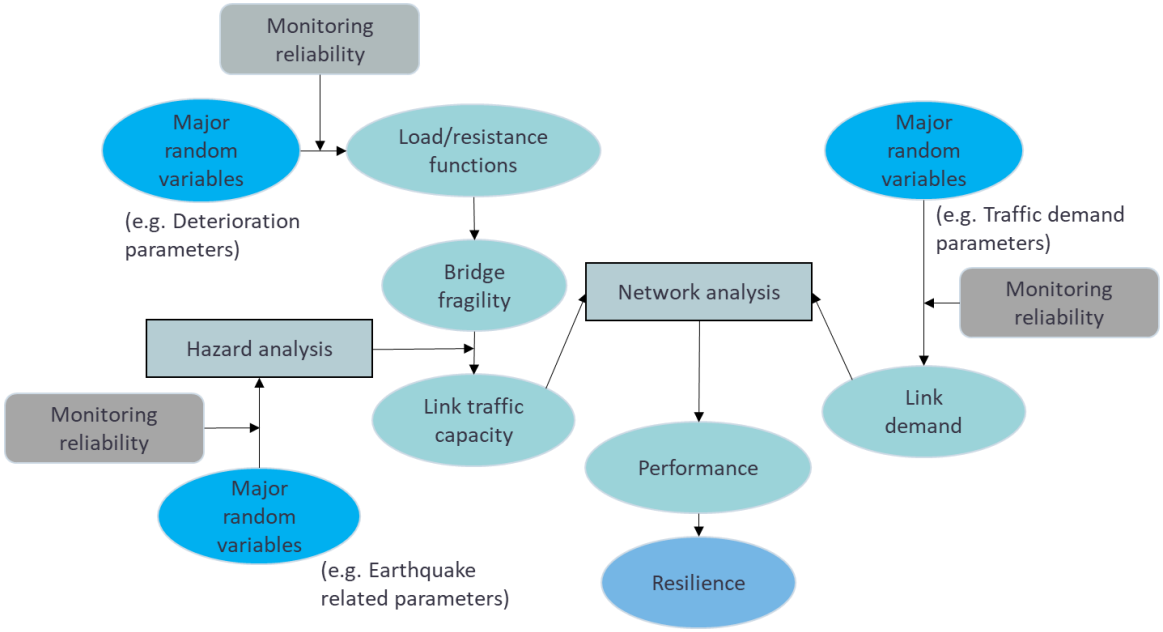

Figure 8. Conceptual representation of a series of probabilistic dependence in the proposed resilience assessment model

Information entropy is used to quantify uncertainties in the PDFs of random variables in resilience assessment. Specifically, in this project, information entropy is used to quantitatively assess the

effect of additional field measurement data on the reduction of uncertainties in resilience assessment. In classical physics, entropy is a measure of the quantity of energy that is no longer available to do physical work. Shannon (1948) extended the entropy concept to information theory to quantify the amount of information as follows:

$$I(x_i) = -\log(p_i) \tag{18}$$

where $I(\cdot)$ = the amount of information; X = the random variable; and p = the probability distribution of X. The value $I(\cdot)$ indicates how much information there is in a random variable X. For example, an event having a lower probability has more information than common events and thus has a higher value of information entropy. On the other hand, there is no information content in a certain or deterministic event. The information entropy, which is also called Shannon entropy, is the expected amount of information in a random variable and is calculated by the following equation (Parhizkar et al., 2018):

$$H(x) = E[I(X)] \tag{19}$$

The information entropy for a discrete random variable X is expressed by:

$$H(x) = \sum_{i=1}^{n} p_i\, I(x_i) = -\sum_{i=1}^{n} p_i \log(p_i) \tag{20}$$

Similarly, the information entropy for a continuous random variable X is defined as:

$$H(x) = -\int f(x) \log\big(f(x)\big)\, dx \tag{21}$$

If observed data (y) on structural capacity and environmental/service conditions are available from inspection and field instrumentations, the cross entropy between the prior and posterior distributions is "a measure of the expected information" that is required to get from the prior distribution to the posterior one (Oladyshkin & Nowak, 2019):

$$H[f(x|y), f(x)] = -\int f(x|y) \log\big(f(x)\big)\, dx \tag{22}$$

To better measure the difference between these two probability distributions, relative entropy (or

Kullback-Leibler divergence), D_{KL}, can be calculated as follows (Oladyshkin and Nowak, 2019):

$$D_{KL}[f(x|y), f(x)] = -H[f(x|y), f(y|x)] \tag{23}$$

Chapter 4. Benchmark Problem

4.1 Overview

In this chapter, the proposed resilience assessment framework is illustrated with a highway network in South Carolina which was previously used as a case study in Rokneddin et al. (2014). This network is selected as a benchmark problem in this study because the surrogate seismic fragility curves of various types of bridges located in the network are available (Ghosh, 2013), which allows us not to develop the surrogate models on our own through extensive structural analyses. As indicated in Rokneddin et al. (2014), the network consists of bridges that are vulnerable to earthquake activity due to a lack of seismic design and retrofit. The bridges in the network are also potentially exposed to marine chloride due to their proximity to the Atlantic Ocean as shown in Figure 9, which makes these bridges more vulnerable to earthquakes over time.

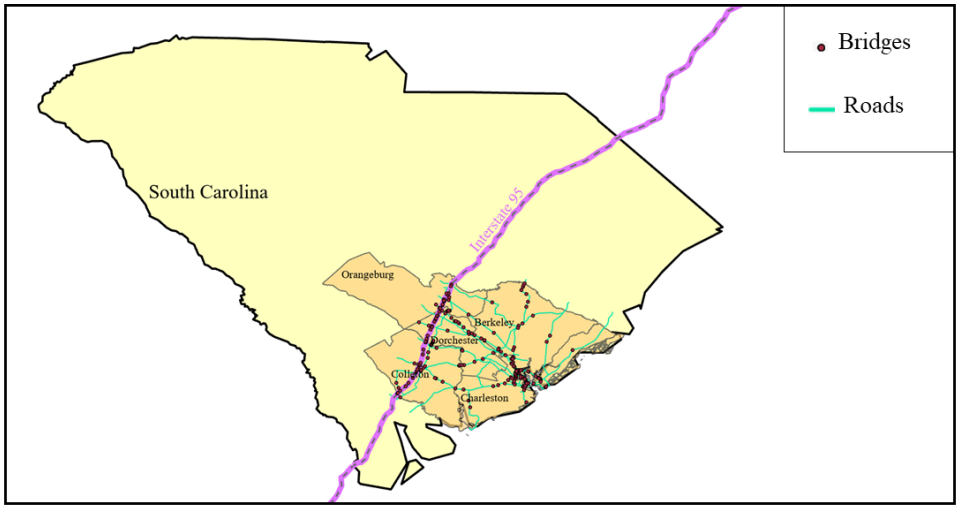

Figure 9. The geographic distribution of the highway network

For the purpose of illustration, a scenario-based approach is taken in this study to quantify and reduce uncertainties along the process of resilience assessment using information entropy and

dynamic BN. Earthquake-related uncertainties are not considered in this benchmark problem because (a) these uncertainties are more like irreducible aleatory uncertainties and (b) probabilistic seismic hazard analysis may require additional computational burden. It should be noted that uncertainties in the earthquake hazard intensity, location, frequency, and timing can be quantified by following the same procedure that will be introduced for other random variables (chloride concentration and traffic demand) in the remaining chapter. The scenario earthquake event considered is the 1886 Charleston earthquake, one of the most damaging earthquakes in the eastern United States. Its estimated moment magnitude was 6.9 – 7.3 Mw, and over 2,000 buildings were damaged.

Information about the bridges in this network is obtained from the national bridge inventory database. Based on the number of spans, major construction materials, and types of design/construction, the bridges are broadly categorized into five different classes as shown in Table 4. Table 4 also shows the inventory of bridges in the case study region. Figure 10 details the age distribution of the bridges in the case study region. According to the study conducted by Ghosh (2013), it was identified that bridges in this case study region constructed before 1990 are lacking seismic detailing. The bridges are also classified into two categories based on their proximity to the ocean: marine splash zone for the bridges within 10 m of the coastline and marine atmospheric zone for the bridges outside the splash zone.

Table 4. Bridge classification and inventory in the network (adopted from Nielson (2005))

Bridge class	Material	Construction type	Spans	Inventory
BD1- MSSS slab	Concrete Prestressed concrete	Slab	>1	51
BD2-MSSS steel girder	Steel	Stringer Tee-beam Floor girder Channel beam	>1	67

BD3-MSSS concrete girder	Concrete Prestressed concrete	Stringer Tee-beam Floor girder Channel beam	>1	82
BD4-MSC steel girder	Continuous steel	Stringer Tee-beam Floor girder Channel beam	>1	42
BD5-MSC slab	Concrete continuous Prestressed concrete continuous	Slab	>1	45
Total				287

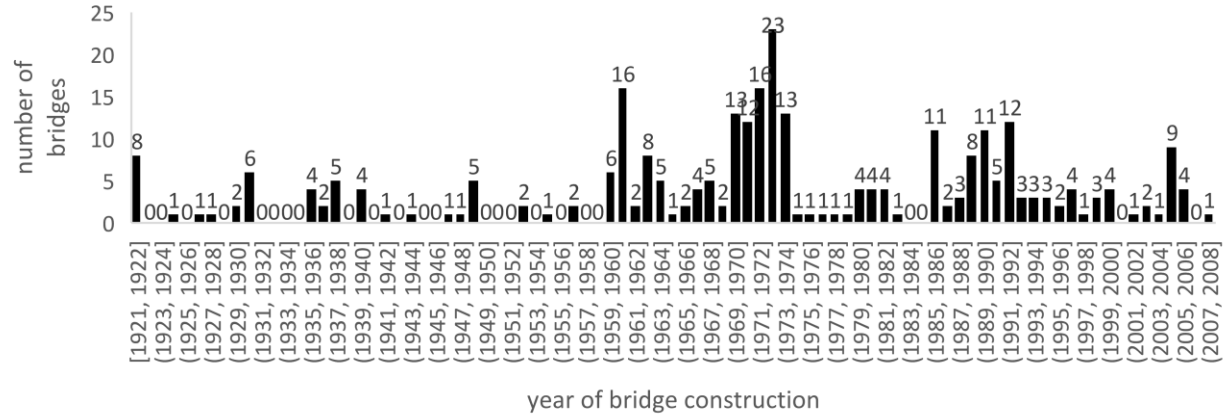

Figure 10. Age distribution of bridges in the case study region

4.2 Dynamic Bayesian Updating with Field Measurement Data

To examine the role of investigating and monitoring major random variables (specifically surface chloride concentration and traffic demand) in resilience assessment, this study considers three cases: (a) Case A: the baseline case where transportation resilience is measured based on the prior distributions of random variables, which is consistent with most existing studies introduced in Chapter 2; (b) Case B: true transportation resilience which is never known in the real world; and (3) Case C: the case where transportation resilience is measured based on the updated posterior distributions of random variables. Figure 11 illustrates the dynamic BN embedded in the proposed seismic resilience assessment, which represents Case C. More specifically, in Case C, it is assumed

that two random variables that change over time – surface chloride concentration and traffic demand – are monitored and that their prior probability distributions are updated over time through dynamic BN.

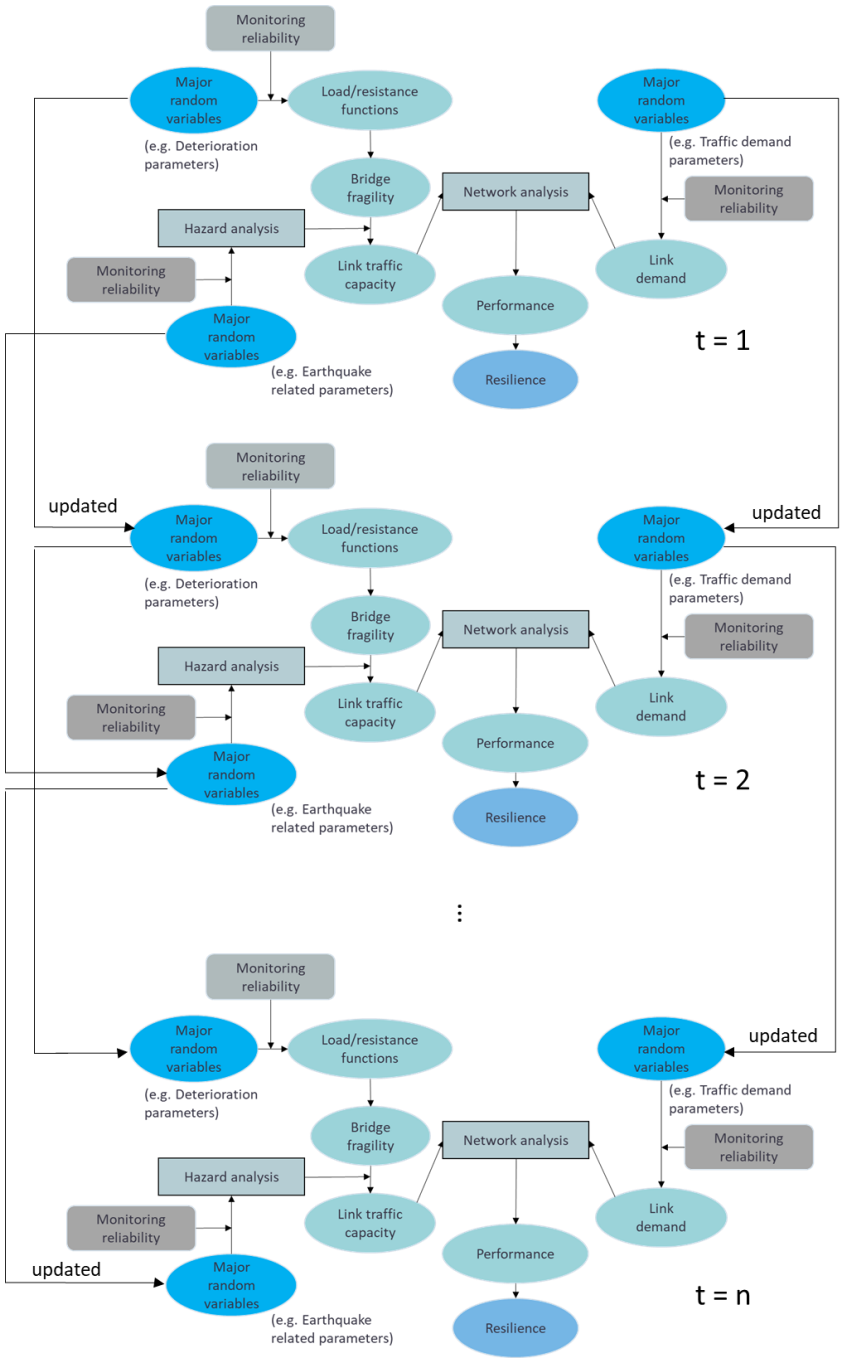

Figure 11. Dynamic Bayesian network embedded in seismic resilience assessment

Input vector (x) and logistic regression coefficients (θ) of the parameterized fragility curve equation (i.e., Equation 12) vary depending on the class of bridge and the provision of seismic detailing. Among them, the area of rebar (x_1) in Table 2 is one of the key parameters and is included in the fragility curves of all bridge classes regardless of its seismic delating. As described in Section 3.1, surface chloride corrosion may induce the reduction in the area of rebar and ultimately affects time-dependent failure probabilities of bridges, which is considered in calculating both bridge and link capacities (see Section 3.2). Therefore, monitoring data on surface chloride corrosion at all bridge locations over time may improve our understanding of time-dependent bridge and network capacity. On the other hand, traffic demand at each highway link also changes over time due to population changes (Zhao et al., 2021), land-use conditions (Faghih-Imani et al., 2014), infrastructure development, intelligent transport system (Kaparias et al., 2012), and policies related to traffic control technologies (e.g., ramp metering, road pricing, route guidance, variable speed limits) (Marchau et al., 2010). Thus, monitoring and updating traffic demand over time may improve the accuracy of network performance assessment. By combining these two time-dependent random variables for all the links in the network, network performance is assessed and updated at every time step.

For Case A, the prior probability distributions of surface chloride concentration for bridges vary depending on bridge location and construction year. Prior knowledge suggests that surface chloride concentration is lognormally distribution with the mean values outlined in Table 5 and a coefficient of variation of 0.5. While these prior distributions consider randomness in C_s, they cannot capture the time-dependent characteristics of chloride concentration as many static resilience assessment studies do.

Table 5. Prior mean values of surface chloride concentration for the bridges based on their location and construction year (adopted from Ghosh, (2013))

Bridge construction year	Marine Atmospheric zone	Marine Splash zone (30 ft (10 m))
	Surface chloride concentration C0(kg/m3) mean value	Surface chloride concentration C0(kg/m3) mean value
1920-1940	2.112	5.28
1941-1960	1.44	4.8
1961-1980	0.96	4.32
1981-2000	0.768	2.88
2000-2008	0.48	1.92

True time-dependent chloride concentrations at the surface (i.e., Case B) are never known in the real world due to epistemic uncertainties. Thus, in this study, we generate synthetic true C_s values by randomly sampling its initial value from the prior distributions shown in Table 5 and applying Equation 24 to generate time-dependent C_s over a 50-year period (Song et al., 2008).

$$C_s(t) = C_0 + \alpha \ln(t) \tag{24}$$

where C_0 = the surface chloride concentration at the beginning; and α = the constant value of 0.6856. The procedure described above, however, does not account for spatial correlation in surface chloride concentration between adjacent locations, which has been identified as one of the factors that may affect the accuracy of time-dependent bridge functionality. To generate spatially correlated chloride concentration values, the Kriging spatial interpolation technique is used. According to the exponential variogram for surface chloride concentration provided in Ghosh (2013), the "range" is 8 km, where semi-variance reaches a plateau and observations are no longer spatially correlated. Therefore, we first divide the entire case study region into 8 km x 8 km cells and randomly generate initial surface chloride concentration at the centroid of each cell. It is because the distance between two centroids is equal to the "range" and initial chloride

concentrations at these centroids are not spatially correlated and can be randomly generated from the prior distributions specified in Table 5. Then, the Kriging technique is used to calculate $C_s(t)$ at the locations between the centroids as illustrated in Figure 12. At the next time step, Equation 24 is applied to generate surface chloride concentration only at the centroids, and then the Kriging technique is used to generate spatially correlated values over the network. This procedure is repeated until the end of 50-year time period.

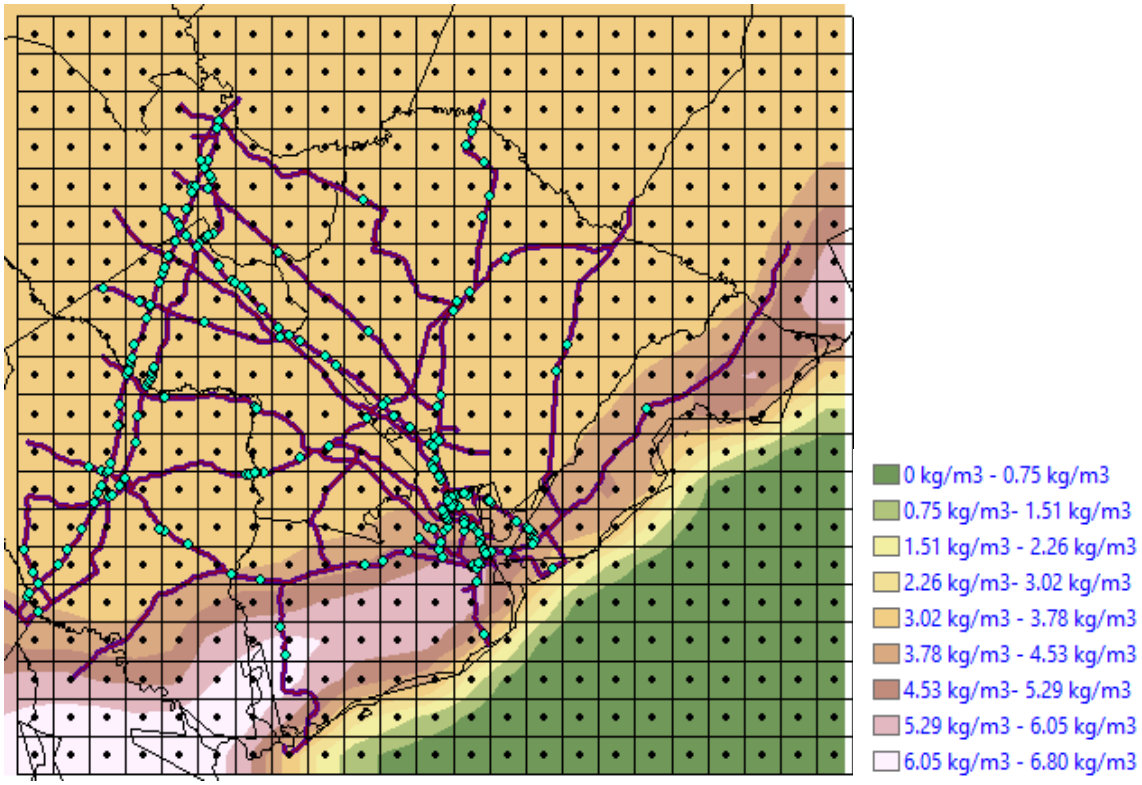

Figure 12. Result from spatial Kriging of surface chloride concentration at Year 50

The time-dependent surface chloride concentration values are used to update the area of rebar at each bridge location (See Equations 3 and 4), which is subsequently used as an input to the time-dependent fragility curve. For Case C, surface chloride concentration values are monitored over time, and Bayesian updating is employed to update the probability distributions and time-dependent fragility curves. In this study, synthetic measurement data are generated. These

plausible measurement-data realizations are generated by combining the true value with a random error term as follows:

$$C_{s,m}(t) = C_{s,t}(t) + \varepsilon_e \tag{25}$$

where $C_{s,m}$ = the time series measurement data; $C_{s,t}(t)$ = the true values or ideal data; and ε_e = the measurement error reflecting our confidence in the measurement data. Given that the true data will never be known exactly, the measurement data can be used to better represent true states of surface chloride concentrations. In this study, the PDFs of surface chloride concentration $P_{C_s}(C_s, t)$ at all bridge locations are updated based on the synthetic measurement data through dynamic Bayesian updating as described in Section 3.5. Subsequently, the posterior PDFs of $P_{C_s}(C_s, t)$ are used to update the time-dependent fragility functions.

Similarly, we generate synthetic values of traffic demand for the three cases. The annual average daily traffic (AADT) data obtained from the South Carolina Department of Transportation (SCDOT) are used to predict the theoretical traffic demands over the next 50 years. SCDOT provides AADT data that have been collected from sensors placed on the road network in the past 17 years. This study specifically uses an autoregressive integrated moving average (ARIMA) model in generating the theoretical values of traffic demands because ARIMA models can (a) capture the seasonality and long-term trends that the AADT data exhibit and (b) provide accurate forecasts for both short- and medium-term AADT predictions. The ARIMA model is mathematically written as:

$$\mathrm{Y}_t = \mathrm{c} + \sum_{i=1}^{p} \phi_i \cdot y(t-i) + \sum_{j=1}^{q} \theta_j \cdot e(t-j) + \mathrm{e}_{\,t} \tag{26}$$

where Y_t = the forecasted value at time t; c = the constant; p = the order of the lag; q = the order of the error lag; ϕ_i = the coefficient of the ith auto regression term; θ_j = the coefficient of the jth moving average term; and e = the error term. In this study, the R software is used in fitting and

forecasting the traffic demand. After generating the theoretical (simulated) values of traffic demand using the ARIMA model, the synthetic true values and synthetic measurement data are generated based on the following equations, respectively:

$$y_t(\boldsymbol{x}) = y_a(\boldsymbol{x}, \boldsymbol{\theta}) + \varepsilon_a \tag{27}$$

$$y_m(\boldsymbol{x}) = y_t(\boldsymbol{x}) + \varepsilon_{obs} \tag{28}$$

where $\boldsymbol{x}$ = the set of independent variables; $y_t(\boldsymbol{x})$ = the synthetic true values of traffic demand; $\boldsymbol{\theta}$ = the set of model parameters; $y_a(\boldsymbol{x}, \boldsymbol{\theta})$ = the outputs of the ARIMA model, that are the theoretical values of traffic demand; ε_a = the modeling error; $y_m(\boldsymbol{x})$ = the synthetic measurement data on traffic demand; and ε_{obs} = the measurement error which is usually modeled as a Gaussian random variable. In general, the measurement error is smaller than the modeling error. To clarify, the theoretical values, $y_a(\boldsymbol{x}, \boldsymbol{\theta})$, are used for traffic demand in Case A, the synthetic true values, $y_t(\boldsymbol{x})$, are used in Case B, and the synthetic measurement data, $y_m(\boldsymbol{x})$, are used in Case C.

Table 6 provides an example of the different accuracies (i.e., measurement errors) of various non-destructive inspection techniques. Non-destructive inspection techniques are widely used to evaluate the condition of transportation infrastructure without causing damage to the structure. The accuracy of these techniques can vary depending on several factors such as the equipment used, the experience of the inspector, and the condition of the structure being evaluated. The reliability of the data obtained from these techniques is crucial for accurate performance and resilience assessment of transportation systems. Inaccurate data can lead to incorrect assessment, which can have serious consequences for the safety and reliability of the transportation system. Therefore, in this project, a sensitivity analysis is performed to evaluate how data reliability affects the accuracy of the estimation of system performance and resilience. By doing so, it is possible to determine the level of confidence in the resilience assessment results and make informed decisions about

maintenance and repair strategies.

Table 6. Non-destructive inspection techniques with varying accuracies (adopted from Atadero et al. (2019))

Non-destructive inspection techniques	Detects/Measures	Accuracy/Precision
Pachometer	Depth of concrete	±15% of cover depth
Chloride Ion Penetration test	Chloride concertation and Diffusion coefficient	±0.0106 % chloride by mass of concrete
Half-cell Potential	Measures the probability of corrosion.	±20 mV
Polarization Resistance	Corrosion Current Density	Stern-Geary Coefficient (25 mv–50 mv) Polarization Resistance with an error factor ±2.83 ohm-cm2

Transportation agencies often rely on consultants to perform monitoring/inspection techniques. However, it is important to note that different consultants may have varying levels of inspection quality, which can impact the accuracy of the data obtained. Table 7 provides an example of the inspection qualities of different consultants. As shown in Table 7, some consultants may produce biased results, which can have serious consequences for the resilience assessment of the transportation system. Specifically, the table shows that consultant 3 underestimates the true value, while consultant 4 overestimates the true value.

Table 7. Different Inspection qualities (adopted from Abdallah et al. (2021))

Consultants	Non-destructive inspection techniques used	Inspection Quality
Consultant 1	Chloride Ion penetration test	Unbiased, with accuracy ±10% out of the measured surface chloride content
Consultant 2	Chloride Ion penetration test	Unbiased, with accuracy ±25% out of the measured surface chloride content

Consultant 3	Chloride Ion penetration test	Biased (real value will be higher than measurement), with accuracy $\pm$10% out of the measured surface chloride content
Consultant 4	Chloride Ion penetration test	Biased (real value will be lower than measurement), with accuracy $\pm$10% out of the measured surface chloride content
Consultant 5	Chloride Ion penetration test	Unbiased, with accuracy $\pm$25% out of the measured surface chloride content
	Cover meter test	Unbiased, with accuracy $\pm$15% out of the measured concrete cover.

In this project, a range of equipment with different accuracies is considered. To simplify the modeling procedure, the coefficient of variation of the modeling error term (ε_{obs} in Equation 28) is chosen as the representative metric, which ranges from 0.05 to 0.3 in increments of 0.05. This range represents the variability in accuracy of the equipment being used.

4.3. Network Analysis and Seismic Resilience Assessment

To perform network analysis, we first determine the capacities and demands of all links in the network. Conditioned on the 1886 Charleston earthquake, a ground motion intensity map in the study region is generated through Open-Source Seismic Hazard Analysis (OpenSHA) (Field et al., 2003). While a set of ground motion intensity maps should be generated for the scenario earthquake to account for uncertainties, only the median values of ground motion intensities are used in this paper for the purpose of simplification. Figure 13 shows the group motion intensity map generated through OpenSHA. By combining the ground motion intensity at every bridge location with the corresponding seismic fragility curves, we can find the failure probabilities of all bridges. It should be noted that these failure probabilities are updated over time because time-dependent fragility curves are updated based on the measurement data.

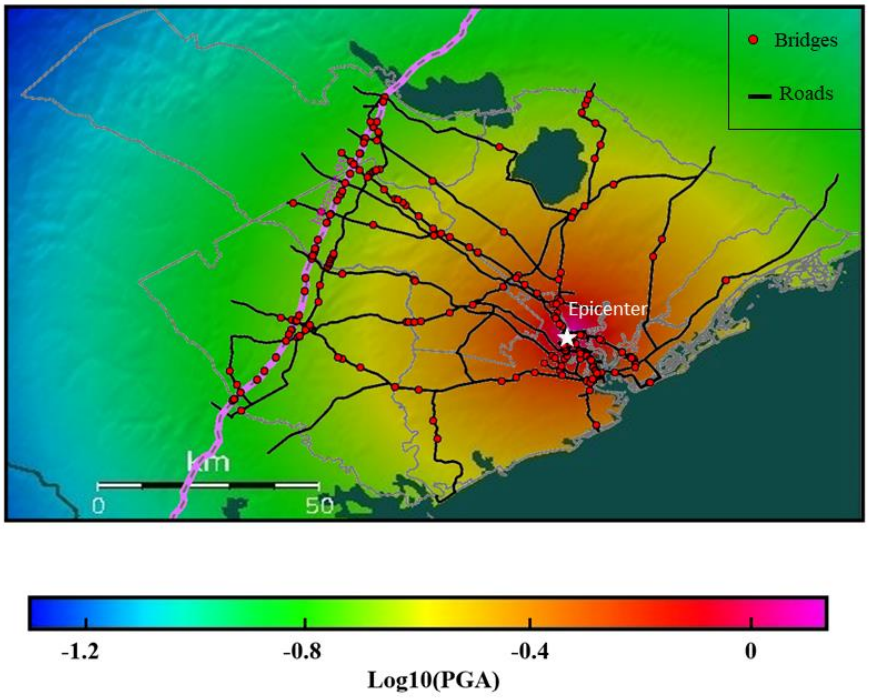

Figure 13. Ground motion intensity map for the study region

The updated probability of failure of each bridge, that is the result of the fragility function, is converted into the reliability index (β). Lee and Ghasemi (2021) proposed a reliability-based indicator for assessing the expected post-earthquake traffic flow capacity of a highway bridge. The relationship between reliability index and post-earthquake traffic carrying capacity (TCC) is shown in Figure 14 as well as in the following equation (Lee & Ghasemi, 2021):

$$TCC = 0.2432e^{0.3548\beta} \tag{29}$$

This study assumes that bridges play a key role in determining transportation network performance and that the bridges on the same link can be modeled as a series system. At every time step, the reliability indices of all bridges are updated based on the measurement data and are converted into their post-earthquake traffic-carrying capacities and the associated link capacities. As described in Section 3.3, the link capacities are used as inputs to the CUBE voyager software program to measure network performance. In addition, the updated traffic demands for all links are also

incorporated into the network analysis so that both updated link capacity and demand affect the performance of the network.

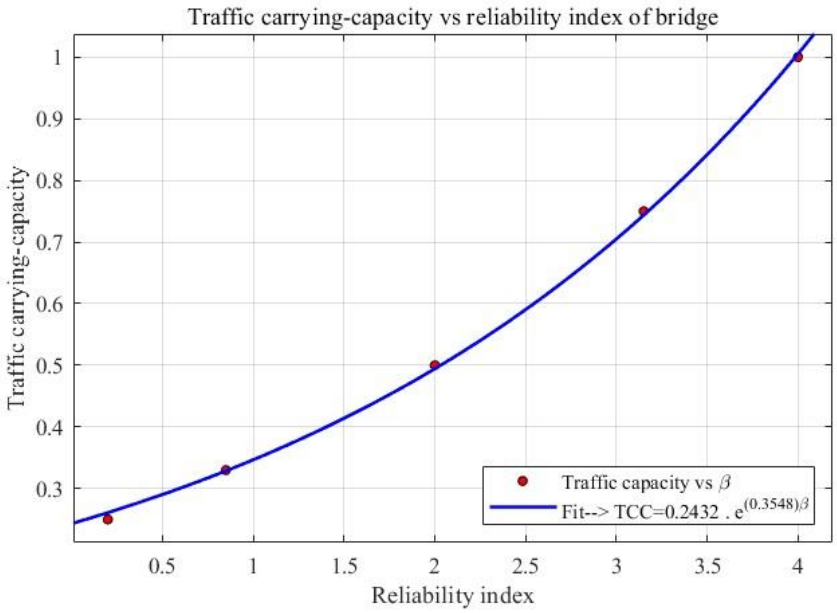

Figure 14. Relationship between reliability index and traffic flow capacity

As described in Section 3.4, the network performance is measured by the total travel time, $TTT(t)$. After the 50-year performance profile of the network is obtained, the time-dependent resilience of the case study network is calculated using Equation 15. Finally, information entropy is calculated by following the procedure described in Section 3.5. The information entropy of each node in the Bayesian network is calculated, and then their sum gives the total information entropy of the system.

Chapter 5. Results and Discussion

To estimate the resilience of a transportation network over time, the parameterized fragility curve equations are considered in this study to estimate the probabilities of failure of the bridges. Figure 15 presents the time-dependent mean chloride concentration values at a specific location for the three cases: the baseline values (Case A), the true values (Case B), and the values updated continuously based on field measurement data (Case C). Case A does not incorporate the temporal variability of chloride concentration, resulting in a constant value over time, as depicted in Figure 15. Conversely, Cases B and C demonstrate an increasing trend over time, which may lead to more severe structural deterioration. While Cases B and C exhibit a similar trend, their discrepancy is observed due to measurement errors (i.e., ε_e in Equation 25). Figure 16 shows the fragility curves of a specific bridge for different years under Case C. The fragility curves are updated over time due to posterior chloride concentration values obtained through dynamic BN. This figure shows how the probability of failure increases with time due to the effect of corrosion-induced deterioration.

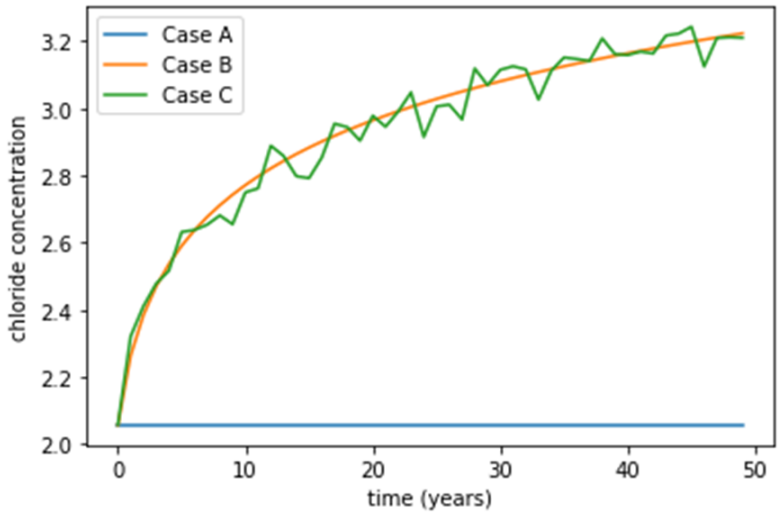

Figure 15. Time-dependent mean chloride values for Cases A, B, and C

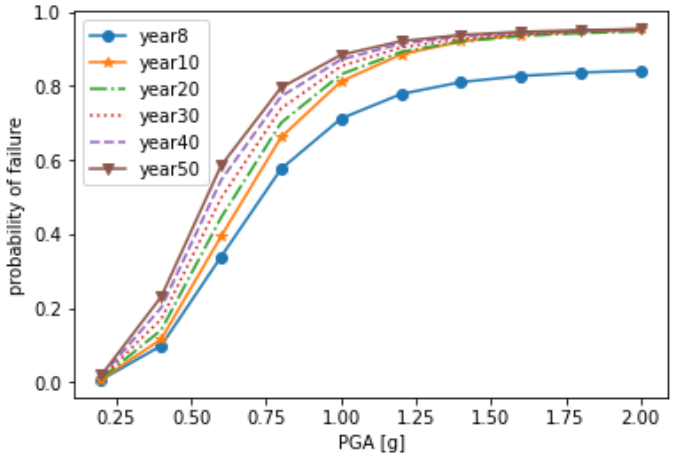

Figure 16. Fragility curves of a specific bridge for different years (Case C)

Figure 17(a) compares the fragility curves of a bridge for Cases A, B, and C at Year 50. This comparison allows for an assessment of the accuracy of the theoretical (Case A) and updated (Case C) values compared to the true values (Case B). The results demonstrate the significance of monitoring and inspection programs in improving the accuracy of bridge fragility assessments. As expected, the fragility curve updated based on field measurement data is much closer to the true fragility curve, which indicates that the proposed dynamic BN method is capable of estimating bridge failure probability in a more accurate manner compared to using only prior theoretical information. Given that true fragility curve is never known in the real world, the proposed model offers a reliable and practical way to improve our knowledge about major deterioration-related random variables and ultimately enhance our prediction about bridge failure probability. Figure 17(b) displays the time-dependent mean traffic demands of a link in the network for the three cases. Similar to Figure 17(a), Case C is much closer to Case B as compared to Case A, highlighting the benefit of monitoring traffic demand over time.

The total travel time for the case study network is estimated using CUBE software, which is a transportation planning software commonly used in evaluating the performance of transportation

networks, analyzing travel demand, and estimating travel time. To estimate the total travel time for the case study network using CUBE while incorporating time-dependent link capacity and demands, CUBE simulates the movement of vehicles and traffic flow through the network over time by taking into account factors such as congestion, signal timing, and speed limits.

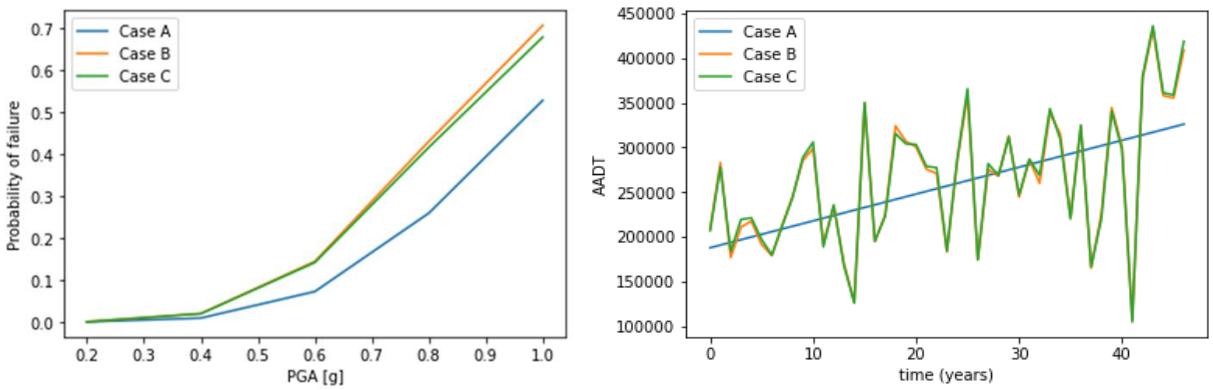

(a) (b)

Figure 17. Comparison between Cases A, B, and C: (a) fragility curves of a bridge at Year 50 and (b) time-dependent mean traffic demand trends at a specific link

The total travel time obtained from the CUBE simulation is incorporated into Equation 16 to evaluate the performance of the case study network. Figure 18 shows time-dependent network performance following the scenario earthquake event at Years 10, 20, 30, 40, and 50. Immediately following the event (at Week 0), there is a significant decrease in network performance due to structural damage to bridges. As recovery activities are initiated, gradual increases in network performance are observed over the next few weeks, ultimately returning to the initial value. Figure 18(a) shows that the overall network performance decreases over time, which is reflected by the decrease in bridge capacity and the increase in traffic demand within the network. Figure 18(b) illustrates a comparison between three cases A, B, and C of the post-earthquake network performance at Year 50. Similar to Figure 17, Cases B and C are closer to each other than Case A because the true values of chloride content and traffic demand are monitored over time in Case C.

In contrast, Case A does not incorporate such monitoring and therefore shows greater deviation from the true values.

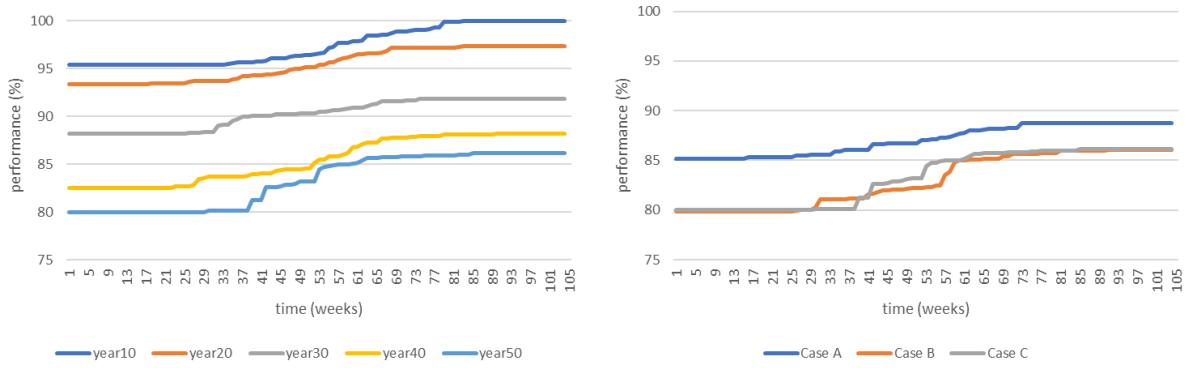

(a) (b)

Figure 18. Time-dependent performance of the network following the scenario earthquake event: (a) Case C at different years and (b) the comparison of Cases A, B, and C at Year 50

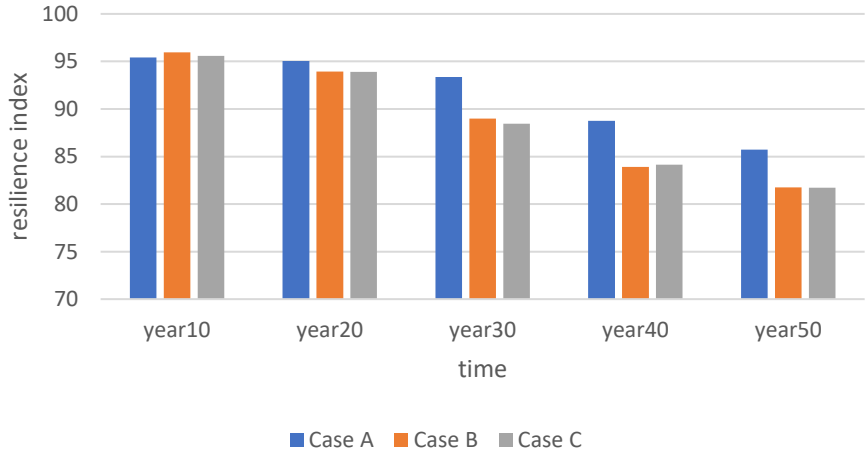

Figure 19. Time-dependent resilience index of the network following the scenario earthquake event: comparison of three cases

Figure 19 shows time-dependent seismic resilience index calculated from Equation 15 following the scenario earthquake event. Overall, the seismic resilience index decreases over time mainly due to bridge deterioration and increased traffic demands. Another finding is that as time increases, the degree of overestimation of network seismic resilience by Case A increases. Conversely, Case C maintains a consistent and accurate estimate of network seismic resilience, even in the distant

future. This also highlights the significance of monitoring and inspection in reducing uncertainties. However, it should be noted that there is some deviation between Cases B and C, which can be attributed to measurement errors. Such errors may occur due to various factors such as equipment limitations, human error, etc. These errors can affect the accuracy of the data and consequently impact the total travel time, network performance, and seismic resilience.

To investigate how the reliability of monitoring and inspection equipment can impact the accuracy of the seismic resilience assessment results for the case study network over time, a sensitivity analysis is performed. A range of equipment with different levels of reliability is included in the sensitivity analysis, with a coefficient of variation (CoV) values of the measurement error term ranging from 0.5 to 3.0. More specifically, the CoV of ε_e in Equation 25 and the CoV of ε_{obs} in Equation 28 vary for chloride concentration and traffic demand, respectively. In the case where the CoV is 0, Case C becomes identical to the true case (i.e., Case B). Figure 20 shows the sensitivity analysis results of network seismic resilience to the reliability of monitoring equipment. The figure compares the 95% confidence intervals of seismic resilience index for the equipment with the highest reliability (i.e., CoV of 0.5) and the lowest reliability (i.e., CoV of 3.0). As expected, the equipment with higher reliability is more accurate in predicting the true seismic resilience index. Thus, by utilizing high reliability monitoring equipment, transportation mangers can obtain more accurate and reliable resilience assessment results, make better informed decisions, and take effective necessary actions to improve the overall seismic resilience of the transportation network. The sensitivity analysis results can further be used to determine the level of monitoring equipment reliability that is required to achieve a desired level of accuracy in the seismic resilience assessment.

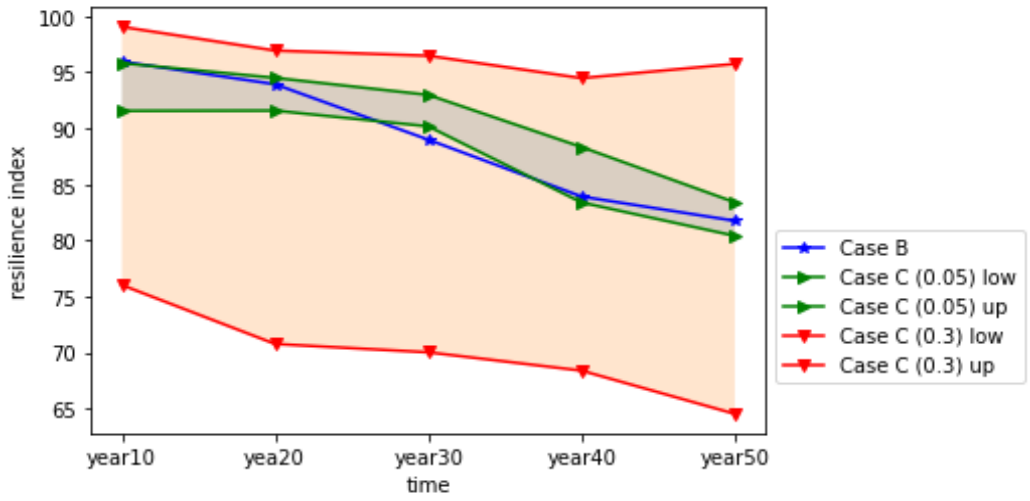

Figure 20. Sensitivity analysis results of network seismic resilience to the reliability of monitoring equipment (95% confidence interval)

To quantify uncertainties along the process of seismic resilience assessment, information entropy values for two monitoring equipment with different levels of reliability (i.e., CoV of 0.05 and CoV of 0.3) are calculated using Equation 21. The results are then used to create Figures 21 and 22. Figures 21(a) and (b) depict geographic maps of information entropy for bridge failure probability at Year 50 when using higher-reliability equipment (CoV of 0.05) and lower-reliability equipment (CoV of 0.3), respectively. Each bridge has a unique information entropy value, which reflects different amounts of randomness or uncertainty. It is found that when lower-reliability equipment is used, the information entropy values for bridge failure probability are higher, indicating a greater degree of uncertainty. Similar observations can be found in Figure 22 that compares information entropy values for traffic demand at Year 50 when it is monitored through higher-reliability equipment (CoV of 0.05) and lower-reliability equipment (CoV of 0.3). Finally, information entropy of seismic resilience index is calculated. Due to the higher values of information entropy for bridge failure probability and traffic demand, the information entropy for seismic resilience index is 21% higher at Year 50 when lower-reliability equipment is used compared to higher-reliability equipment.

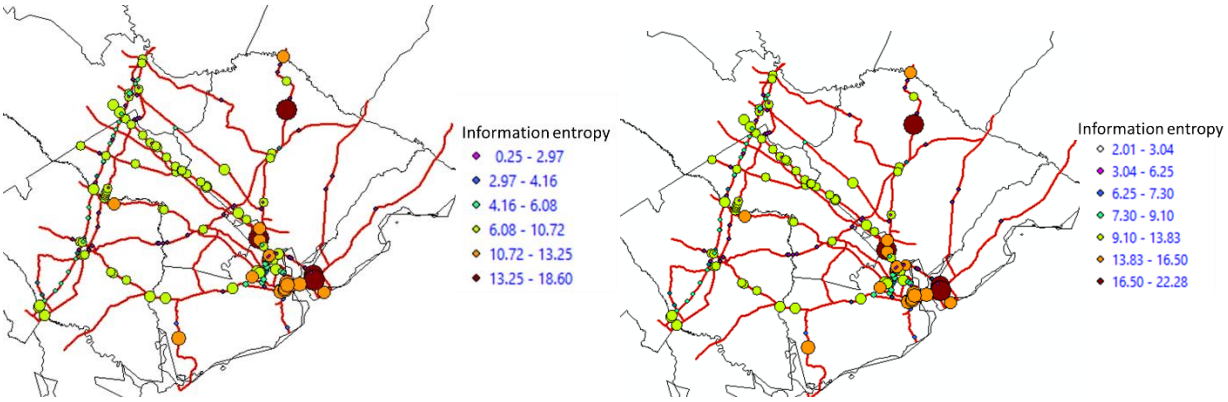

(a) (b)

Figure 21. Geographic distribution of information entropy for bridge failure probability at Year 50: (a) using higher-reliability equipment and (b) using lower-reliability equipment

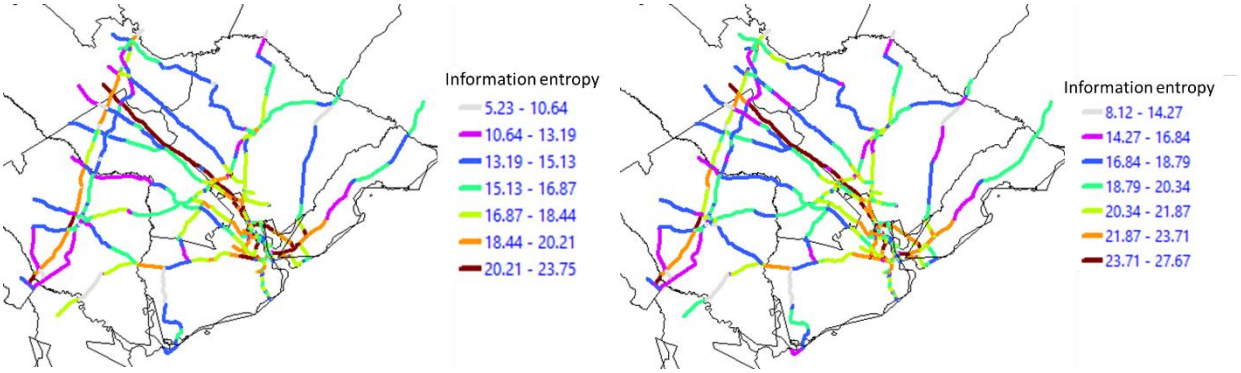

(a) (b)

Figure 22. Geographic distribution of information entropy for traffic demand at Year 50: (a) using higher-reliability equipment and (b) using lower-reliability equipment

Figure 23 presents a percentage increase in information entropy with respect to the baseline value (i.e., Year 10 value) over time. The increase in information entropy over time for both cases suggests an increase in the amount of uncertainty in the process. This is an important finding because it highlights the need to carefully consider the reliability of the monitoring equipment used in seismic resilience assessment to ensure accurate results. Additionally, the slower increase in information entropy over time when using higher-reliability equipment indicates that epistemic

uncertainty decreases more quickly over time, making it an attractive option for long-term seismic resilience assessment.

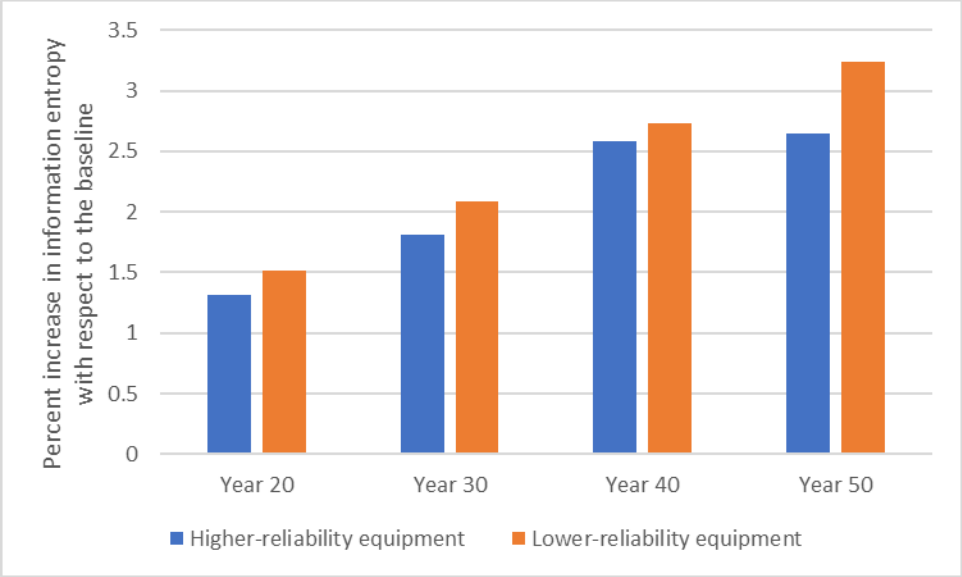

Figure 23. Percentage increase in information entropy with respect to the baseline value (i.e., Year 10 value) over time: higher- and lower-reliability monitoring equipment

Practical applications of these findings include informing decisions about the selection of monitoring equipment for seismic resilience assessment, as well as providing a framework for assessing uncertainties in the process. This information can be used to identify areas that require further investigation or intervention to improve the resilience of transportation network in earthquake-prone regions.

Chapter 6. Summary and Conclusions

This final report presented a dynamic BN-based resilience assessment model for a large-scale transportation network that can explicitly quantify uncertainties in all phases of the assessment and investigate the role of inspection and monitoring programs in uncertainty reduction. First, uncertainties in transportation network capacity and demand were identified and reduced through a dynamic BN based on measurement data collected over time. Subsequently, the updated link capacity and demand were incorporated into network analysis to update seismic resilience over time. The proposed model was then tested on a benchmark problem, a highway network in South Carolina, to demonstrate how the model could systematically quantify and reduce uncertainties when assessing the seismic resilience of the network. To further examine the significance of measurement data in improving the accuracy of prediction of seismic resilience index, a sensitivity analysis was performed using different sets of data with varying accuracies.

The benchmark problem results showed that incorporating monitoring and inspection data on important variables such as chloride concentration and traffic demands could improve predicting the seismic resilience of the network. It also suggested the need to consider equipment reliability when designing monitoring and inspection programs. These findings can assist transportation managers and policymakers in identifying necessary equipment reliability levels and prioritizing inspection and monitoring efforts. The impact of this project is significant as it provides decision-makers with the tools to better manage transportation system resilience in the face of natural hazards and uncertainty. The results can be used to determine which techniques to prioritize, evaluate the effectiveness of current programs, and perform cost-benefit analyses for optimal resource allocation.

References

1. Abdallah, A.M., Atadero, R.A., & Ozbek, M.E. (2021). A comprehensive uncertainty-based framework for inspection planning of highway bridges. *Infrastructures*, 6(2), 27.
2. Adams, T. M., Bekkem, K. R., & Toledo-Durán, E. J. (2012). Freight resilience measures. *Journal of Transportation Engineering*, *138*(11), 1403-1409.
3. Atadero, R. A., Jia, G., Abdallah, A., & Ozbek, M. E. (2019). An Integrated Uncertainty-Based Bridge Inspection Decision Framework with Application to Concrete Bridge Decks. *Infrastructures*, 4(3), 50.
4. Barker, K., Ramirez-Marquez, J. E., & Rocco, C. M. (2013). Resilience-based network component importance measures. *Reliability Engineering & System Safety*, 117, 89-97.
5. Berche, B., Von Ferber, C., Holovatch, T., & Holovatch, Y. (2009). Resilience of public transport networks against attacks. *The European Physical Journal B*, *71*(1), 125-137.
6. Bostick, T. P., Connelly, E. B., Lambert, J. H., & Linkov, I. (2018). Resilience science, policy and investment for civil infrastructure. *Reliability Engineering & System Safety*, *175*, 19-23.
7. Bruneau, M., & Reinhorn, A. (2006). Overview of the resilience concept. In *Proceedings of the 8th US national conference on earthquake engineering* (Vol. 2040, pp. 18-22).
8. Bruneau, M., Chang, S. E., Eguchi, R. T., Lee, G. C., O'Rourke, T. D., Reinhorn, A. M., ... & Von Winterfeldt, D. (2003). A framework to quantitatively assess and enhance the seismic resilience of communities. *Earthquake spectra*, *19*(4), 733-752.
9. Bu, L., Qiao, L., Sun, R., Lu, W., Guan, Y., Gao, N., ... & Qin, Y. (2022). Time and crack width dependent model of chloride transportation in engineered cementitious composites (ECC). *Materials*, *15*(16), 5611.

10. Castillo, E., Grande, Z., & Calviño, A. (2016). Bayesian networks-based probabilistic safety analysis for railway lines. *Computer-Aided Civil and Infrastructure Engineering*, 31(9), 681-700.
11. Chang, S. E., & Shinozuka, M. (2004). Measuring improvements in the disaster resilience of communities. *Earthquake spectra*, *20*(3), 739-755.
12. Chen, A., Kasikitwiwat, P., & Yang, C. (2013). Alternate capacity reliability measures for transportation networks. *Journal of Advanced Transportation*, *47*(1), 79-104.
13. Coronelli, D., & Gambarova, P. (2004). Structural assessment of corroded reinforced concrete beams: modeling guidelines. *Journal of structural engineering*, *130*(8), 1214-1224.
14. Cox, A., Prager, F., & Rose, A. (2011). Transportation security and the role of resilience: A foundation for operational metrics. *Transport policy*, *18*(2), 307-317.
15. Czarnecki, A. A., & Nowak, A. S. (2008). Time-variant reliability profiles for steel girder bridges. *Structural Safety*, *30*(1), 49-64.
16. Du, Y. G., Clark, L. A., & Chan, A. H. C. (2005). Residual capacity of corroded reinforcing bars. *Magazine of Concrete Research*, *57*(3), 135-147.
17. Ellingwood, B. R. (1996). Reliability-based condition assessment and LRFD for existing structures. *Structural Safety*, *18*(2-3), 67-80.
18. Faghih-Imani, A., Eluru, N., El-Geneidy, A. M., Rabbat, M., & Haq, U. (2014). How land-use and urban form impact bicycle flows: evidence from the bicycle-sharing system (BIXI) in Montreal. *Journal of transport geography*, *41*, 306-314.

19. Field, E. H., T. H. Jordan, & C. A. Cornell. (2003). OpenSHA: A Developing community-modeling environment for seismic hazard analysis, *Seismological Research Letters 74*, 406-419.
20. Frangopol, D. M., & Nakib, R. (1991). Redundancy in highway bridges. *Engineering Journal*, *28*(Discussion Paper 115).
21. Ganin, A. A., Kitsak, M., Marchese, D., Keisler, J. M., Seager, T., & Linkov, I. (2017). Resilience and efficiency in transportation networks. *Science Advances*, 3(12), e1701079.
22. Ghasemi, S. H., & Lee, J. Y. (2021). Reliability-based indicator for post-earthquake traffic flow capacity of a highway bridge. *Structural Safety*, 89, 102039.
23. Ghosh, J. (2013). Parameterized Seismic Fragility Assessment and Life-Cycle Analysis of Aging Highway Bridges (Doctoral dissertation, Rice University).
24. Ghosh, J. (2021). Next generation fragility functions for seismically designed highway bridges in moderate seismic zones. *Natural Hazards Review*, 22(1), 04020051.
25. Ghosh, J., Rokneddin, K., Padgett, J. E., & Dueñas-Osorio, L. (2014). Seismic reliability assessment of aging highway bridge networks with field instrumentation data and correlated failures, I: Methodology. *Earthquake Spectra*, *30*(2), 795-817.
26. Gong, C., & Frangopol, D. M. (2020). Condition-Based Multiobjective Maintenance Decision Making for Highway Bridges Considering Risk Perceptions. *Journal of Structural Engineering*, *146*(5), 04020051.
27. Hosseini, S., & Barker, K. (2016). Modeling infrastructure resilience using Bayesian networks: A case study of inland waterway ports. *Computers & Industrial Engineering*, 93, 252-266.

28. Ip, W. H., & Wang, D. (2009, April). Resilience evaluation approach of transportation networks. In *2009 International Joint Conference on Computational Sciences and Optimization* (Vol. 2, pp. 618-622). IEEE.
29. John, A., Yang, Z., Riahi, R., & Wang, J. (2016). A risk assessment approach to improve the resilience of a seaport system using Bayesian networks. *Ocean Engineering*, 111, 136-147.
30. Kammouh, O., Gardoni, P., & Cimellaro, G. P. (2020). Probabilistic framework to evaluate the resilience of engineering systems using Bayesian and dynamic Bayesian networks. *Reliability Engineering & System Safety*, 198, 106813.
31. Kanti Sen, M., & Dutta, S. (2020). An Integrated GIS-BBN Approach to Quantify Resilience of Roadways Network Infrastructure System against Flood Hazard. *ASCEASME Journal of Risk and Uncertainty in Engineering Systems, Part A: Civil Engineering*, 6(4), 04020045.
32. Kaparias, I., Eden, N., Tsakarestos, A., Gal-Tzur, A., Gerstenberger, M., Hoadley, S., ... & Bell, M. (2012). Development and application of an evaluation framework for urban traffic management and Intelligent Transport Systems. *Procedia-Social and Behavioral Sciences*, *48*, 3102-3112.
33. Kezhiyur, A. J. (2015). Analysis of Age-dependent resilience for a highway network with aging bridges. (Master's thesis, Pennsylvania State University). Retrieved from https://etda.libraries.psu.edu/files/final_submissions/10776
34. Lee, H. S., & Cho, Y. S. (2009). Evaluation of the mechanical properties of steel reinforcement embedded in concrete specimen as a function of the degree of reinforcement corrosion. *International Journal of Fracture*, *157*(1), 81-88.

35. Liao, T. Y., Hu, T. Y., & Ko, Y. N. (2018). A resilience optimization model for transportation networks under disasters. *Natural Hazards*, 93(1), 469-489.
36. Mackie, K. R., & Stojadinović, B. (2006). Post-earthquake functionality of highway overpass bridges. *Earthquake Engineering & Structural Dynamics*, *35*(1), 77-93.
37. Madni, A. M., & Jackson, S. (2009). Towards a conceptual framework for resilience engineering. *IEEE Systems Journal*, *3*(2), 181-191.
38. Marchau, V.A., Walker, W.E. and Van Wee, G.P., 2010. Dynamic adaptive transport policies for handling deep uncertainty. *Technological Forecasting and Social Change*, *77*(6), pp.940-950.
39. Meerow, S., Newell, J. P., & Stults, M. (2016). Defining urban resilience: A review. *Landscape and Urban Planning*, *147*, 38-49.
40. Miller-Hooks, E., Zhang, X., & Faturechi, R. (2012). Measuring and maximizing resilience of freight transportation networks. *Computers & Operations Research*, *39*(7), 1633-1643.
41. Molina, F. J., Alonso, C., & Andrade, C. (1993). Cover cracking as a function of rebar corrosion: Part 2—Numerical model. *Materials and Structures*, *26*(9), 532-548.
42. Murray-Tuite, P. M. (2006). A comparison of transportation network resilience under simulated system optimum and user equilibrium conditions. *Proceedings of the 2006 Winter Simulation Conference*. IEEE.
43. Naeemi, A. H., & Albrecht, P. (1984, June). Atmospheric Corrosion of Weathering Steel. In *International Congress on Metallic Corrosion,* (Vol. 1, pp. 418-427).
44. Nielson, B. G. (2005). Analytical fragility curves for highway bridges in moderate seismic zones. (Doctoral dissertation, Georgia Institute of Technology).
45. Nowak, A. S., & Collins, K. R. (2012). *Reliability of structures*. CRC press.

46. Oladyshkin, S., & Nowak, W. (2019). The connection between Bayesian inference and information theory for model selection, information gain and experimental design. *Entropy*, *21*(11), 1081.
47. Ouyang, M., Dueñas-Osorio, L., & Min, X. (2012). A three-stage resilience analysis framework for urban infrastructure systems. *Structural Safety*, *36*, 23-31.
48. Padgett, J. E., & DesRoches, R. (2007). Bridge functionality relationships for improved seismic risk assessment of transportation networks. *Earthquake Spectra*, *23*(1), 115-130.
49. Parhizkar, T., Balali, S., & Mosleh, A. (2018). An entropy based bayesian network framework for system health monitoring. *Entropy*, *20*(6), 416.
50. Rokneddin, K., Ghosh, J., Dueñas-Osorio, L., & Padgett, J. E. (2014). Seismic reliability assessment of aging highway bridge networks with field instrumentation data and correlated failures, II: Application. *Earthquake Spectra*, 30(2), 819-843.
51. Shannon, C. (1948). Claude Shannon. *Information Theory*, *3*, 224.
52. Shiraki, N., Shinozuka, M., Moore, J. E., Chang, S. E., Kameda, H., & Tanaka, S. (2007). System risk curves: Probabilistic performance scenarios for highway networks subject to earthquake damage. *Journal of Infrastructure Systems*, *13*(1), 43-54.
53. Song, H. W., Lee, C. H., & Ann, K. Y. (2008). Factors influencing chloride transport in concrete structures exposed to marine environments. *Cement and Concrete Composites*, *30*(2), 113-121.
54. Stewart, M. G., & Rosowsky, D. V. (1998). Time-dependent reliability of deteriorating reinforced concrete bridge decks. *StructuralSsafety*, *20*(1), 91-109.
55. Thoft-Christensen, P., Jensen, F. M., Middleton, C. R., & Blackmore, A. (1996). Assessment of the reliability of concrete slab bridges.

56. Vecchio, F. J., & Collins, M. P. (1993). Compression response of cracked reinforced concrete. *Journal of Structural Engineering*, *119*(12), 3590-3610.

57. Vugrin, E. D., Warren, D. E., & Ehlen, M. A. (2011). A resilience assessment framework for infrastructure and economic systems: Quantitative and qualitative resilience analysis of petrochemical supply chains to a hurricane. *Process Safety Progress*, *30*(3), 280-290.

58. Zhang, W., Wang, N., Nicholsonc, C., & Tehrani, M. H. (2018). A Stage-wise Decision Framework for Transportation Network Resilience Planning. *arXiv preprint arXiv:1808.03850*.

59. Zhang, X., Miller-Hooks, E., & Denny, K. (2015). Assessing the role of network topology in transportation network resilience. *Journal of Transport Geography*, 46, 35- 45.

60. Zhao, J., Lee, J.Y., & Wolcott, M.P. (2022). Multi-component resilience assessment framework for transportation systems. *Proceedings of the 13th International Conference on Structural Safety and Reliability*, Shanghai, China, June, 2021

61. Zhou, Y., Wang, J., & Yang, H. (2019). Resilience of transportation systems: concepts and comprehensive review. *IEEE Transactions on Intelligent Transportation Systems*, 20(12), 4262-4276.